© 2014. Published by The Company of Biologists Ltd | Journal of Cell Science (2014) 127, 828–844 doi:10.1242/jcs.137802

RESEARCH ARTICLE

Annexin A2 mediates secretion of collagen VI, pulmonary elasticity and apoptosis of bronchial epithelial cells

MaryAnn Dassah[1], Dena Almeida[1], Rebecca Hahn[2,*], Paolo Bonaldo[3], Stefan Worgall[4,5] and Katherine A. Hajjar[1,‡]

ABSTRACT

The annexins are an evolutionarily conserved family of phospholipid-binding proteins of largely unknown function. We observed that the *AnxA2*$^{-/-}$ lung basement membrane specifically lacks collagen VI (COL6), and postulated that ANXA2 directs bronchial epithelial cell secretion of COL6, an unusually large multimeric protein. COL6 serves to anchor cells to basement membranes and, unlike other collagens, undergoes multimerization prior to secretion. Here, we show that *AnxA2*$^{-/-}$ mice have reduced exercise tolerance with impaired lung tissue elasticity, which was phenocopied in *Col6a1*$^{-/-}$ mice. *In vitro*, *AnxA2*$^{-/-}$ fibroblasts retained COL6 within intracellular vesicles and adhered poorly to their matrix unless ANXA2 expression was restored. *In vivo*, *AnxA2*$^{-/-}$ bronchial epithelial cells underwent apoptosis and disadhesion. Immunoprecipitation and immunoelectron microscopy revealed that ANXA2 associates with COL6 and the SNARE proteins SNAP-23 and VAMP2 at secretory vesicle membranes of bronchial epithelial cells, and that absence of ANXA2 leads to retention of COL6 in a late-Golgi, VAMP2-positive compartment. These results define a new role for ANXA2 in the COL6 secretion pathway, and further show that this pathway establishes cell–matrix interactions that underlie normal pulmonary function and epithelial cell survival.

KEY WORDS: Annexin A2, Collagen VI, Secretion

INTRODUCTION

The basement membrane is an electron-dense, 50- to 100-nm-thick, sheet-like structure composed of intricately assembled extracellular matrix proteins that separate epithelial cell monolayers from their underlying connective tissue (LeBleu et al., 2007). Not only do basement membranes provide structural support and serve as barriers to toxins and pathogens, they also provide a conduit for signaling and mechanotransduction (Bateman et al., 2009; Lu et al., 2011). Polarized epithelial cells, such as those in the lung, continuously remodel the basement membrane by secreting and proteolyzing its component proteins; in turn, basement membrane proteins support epithelial cell-adhesion, survival and differentiation (Pozzi and Zent, 2011). Alterations in basement membrane composition accompany an array of human lung disorders, including asthma, chronic obstructive pulmonary disease and interstitial fibrosis (Cox and Erler, 2011; Kranenburg et al., 2006; Lambrecht and Hammad, 2012; Proud and Leigh, 2011).

Most basement membranes consist of a collagen IV and laminin superstructure, whose stability and compliance are refined by expression of additional proteins (LeBleu et al., 2007). In the lung, the basement membrane scaffolding is buttressed by agrin, fibulin, netrin, nidogen, perlecan, tropoelastin (Manabe et al., 2008) and collagen VI (COL6), which together impart elasticity, mechanical support and signaling capability to the bronchial wall (Bober et al., 2010; Gelse et al., 2003; Specks et al., 1995). COL6, a microfibrillar collagen, forms filaments that anchor basement membranes to other collagen fibers (Bonaldo et al., 1990; Engvall et al., 1986; Keene et al., 1988). Abnormalities in COL6 lead to myopathy in the mouse (Bonaldo et al., 1998; Irwin et al., 2003) and zebrafish (Telfer et al., 2010), and to Ullrich and Bethlem congenital muscular dystrophy in humans (Baker et al., 2005; Bönnemann, 2011).

Many basement membrane polypeptides undergo intracellular synthesis and maturation, followed by extracellular assembly (LeBleu et al., 2007). Laminin, for example, consists of polypeptide chains that form intracellular αβγ trimers (~800 kDa), which aggregate into a hexagonal polymer only after secretion (LeBleu et al., 2007). Nidogen and perlecan are secreted without prior complex formation (LeBleu et al., 2007). Collagen IV, which accounts for about 50% of most basement membrane protein mass, assembles into triple helical, kilodalton-scale protomers (~500 kDa), which are also secreted before extracellular assembly into a stable network (Gelse et al., 2003). This is similar to many other collagens that form classical fibrils (Tooley et al., 2010). However, in sharp contrast, COL6 undergoes extensive intracellular assembly of highly crosslinked megadalton-scale 12-subunit complexes (~2000 kDa), which then, upon secretion, associate into a microfibrillar network (Bateman et al., 2009; Colombatti et al., 1995; Engvall et al., 1986).

Annexin A2 (ANXA2), a component of a cell surface fibrinolytic receptor complex (Dassah et al., 2009; Flood and Hajjar, 2011), belongs to a family of conserved, membrane-binding proteins that has been implicated in intracellular membrane-fusion events (Gerke et al., 2005). Intracellularly, ANXA2 and S100A10 form a heterotetramer, which appears to have a calcium-regulated membrane-bridging function. In cultured cells, ANXA2 regulates secretion of surfactant-containing lamellar bodies in the type II

[1]Department of Cell and Developmental Biology, Weill Cornell Medical College, 1300 York Avenue, New York, NY 10065, USA. [2]Department of Medicine, Weill Cornell Medical College, 1300 York Avenue, New York, NY 10065, USA. [3]Department of Molecular Medicine, University of Padova, Viale U. Bassi 58/B I-35131, Padova, Italy. [4]Department of Pediatrics, Weill Cornell Medical College, 1300 York Avenue, New York, NY 10065, USA. [5]Department of Genetic Medicine, Weill Cornell Medical College, 1300 York Avenue, New York, NY 10065, USA.

*Present address: Department of Medicine, Columbia University Medical Center, 161 Fort Washington Avenue, New York, NY 10032, USA.

‡Author for correspondence (khajjar@med.cornell.edu)

Received 1 July 2013; Accepted 19 November 2013

Journal of Cell Science

Journal of Cell Science (2014) 127, 828–844 doi:10.1242/jcs.137802

pneumocyte (Wang et al., 2007), release of catecholamines from dense core vesicles in adrenal chromaffin cells (Umbrecht-Jenck et al., 2010), and exocytosis of ultra-large von Willebrand factor multimers from endothelial cell Weibel–Palade bodies (Knop et al., 2004). In these processes, ANXA2 appears *in vitro* to crosslink secretory granules to the plasma membrane by interacting with soluble N-ethylmaleimide-sensitive factor acceptor proteins 23 and 25 (SNAP-23 and SNAP-25), as well as vesicle associated membrane protein 2 (VAMP2), which are both components of the SNAP receptor (SNARE) complex (Nakata et al., 1990; Umbrecht-Jenck et al., 2010; Wang et al., 2007).

On the basis of previous findings that implicate ANXA2 in membrane-fusion events *in vitro*, we sought to define the role of ANXA2 in basement membrane secretion *in vivo*, and its physiological relevance. We noted that *AnxA2*$^{-/-}$ mice exhibit reduced exercise tolerance and abnormal pulmonary stiffness. Examination of lung tissue from resting mice revealed dysmorphic bronchial epithelial cells, high-level apoptosis and cell dropout. Specific absence of COL6 within the *AnxA2*$^{-/-}$ basement membrane correlated with retention of COL6 bronchial epithelial cell secretory vesicles. In cultured *AnxA2*$^{-/-}$ fibroblasts, secretion of COL6 was impaired, and COL6 was retained within a late-Golgi, VAMP2-positive compartment. By immunoelectron microscopy and immunoprecipitation, ANXA2 and COL6 were identified to be associated with VAMP2 and SNAP-23 within a secretory vesicle membrane complex. Interestingly, skeletal muscle from *AnxA2*$^{-/-}$ mice also demonstrated accumulation of COL6 in the interstitium, its site of synthesis. Together, these data show that ANXA2 enables the specific secretion of COL6, and that absence of ANXA2 leads to epithelial cell dropout, apoptosis and a physiologically significant restrictive pulmonary ventilatory defect.

RESULTS

Impaired exercise tolerance identified in *AnxA2*$^{-/-}$ mice

When littermate mice were enrolled in an exercise protocol consisting of daily 90 minute swims over a 3 week period, *AnxA2*$^{-/-}$ mice exhibited significantly longer post-swim recovery times (49.2±3.5 versus 70.5±7.8 minutes; mean ± s.e., $n=5$ per group, $P=0.018$; Fig. 1A). Compared with *AnxA2*$^{+/+}$ mice, *AnxA2*$^{-/-}$ mice from five separate heterozygous matings showed reduced post-exercise grooming activity and distinctly longer times to complete drying (Fig. 1B). Evaluation of cardiac function by M-mode echocardiography revealed no significant difference in resting heart rate or cardiac output, and heart-to-body-mass ratios at baseline and post exercise did not differ between the two genotypes (not shown). Upon evaluation of pulmonary biomechanics, however, *AnxA2*$^{-/-}$ mice showed significant decreases in both dynamic and static compliance (Fig. 1C,D; $P<0.0001$), and corresponding increases in both

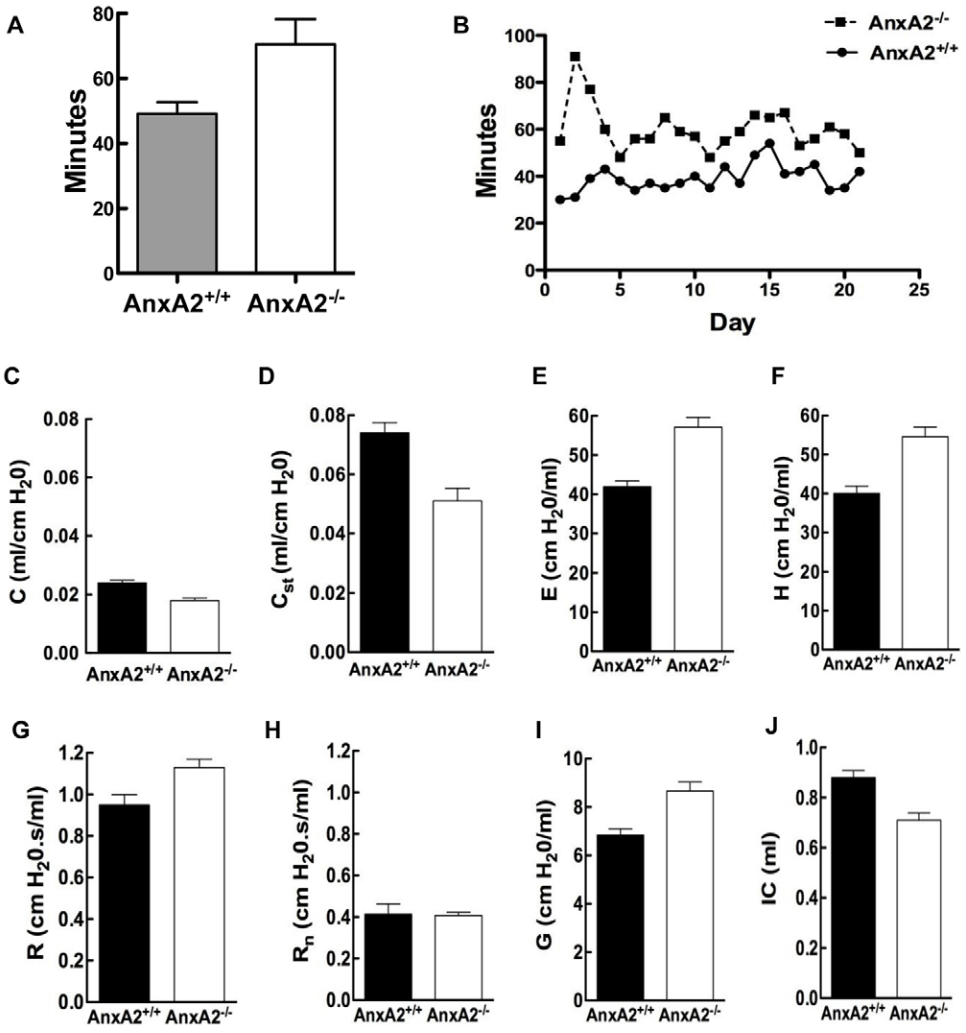

Fig. 1. ANXA2 deficiency is associated with reduced exercise tolerance and a restrictive ventilatory defect. (A) Post-swim recovery times, measured as time to complete dryness for trained littermate *AnxA2*$^{+/+}$ and *AnxA2*$^{-/-}$ mouse pairs averaged over 21 days. Shown are means ± s.e., $n=5$. (B) Post-swim recovery times over 21 days for a single *AnxA2*$^{+/+}$ and *AnxA2*$^{-/-}$ littermate pair mice after swimming. (C–I) Lung biomechanics in *AnxA2*$^{+/+}$ and *AnxA2*$^{-/-}$ mice, including dynamic (C) and static (D) compliance, whole-lung (E) and tissue (F) elastance, total dynamic (G) and airway (H) resistance, tissue dampening (I) and inspiratory capacity (J). $P<0.0001$ for all biomechanical studies, except H, where $P=0.732$ ($n=10$ for all groups).

Journal of Cell Science (2014) 127, 828–844 doi:10.1242/jcs.137802

whole lung and tissue elastance (Fig. 1E,F; $P<0.0001$). Total dynamic resistance was also increased in the *AnxA2*$^{-/-}$ lung (Fig. 1G; $P<0.0001$), whereas airway resistance showed no significant change (Fig. 1H; $P=0.732$), even following increasing doses of methacholine (supplementary material Fig. S1A). Tissue dampening, finally, was increased (Fig. 1I; $P<0.0001$), whereas inspiratory capacity was significantly reduced (Fig. 1J; $P<0.0001$). Together, these data indicated significantly increased tissue stiffness and ventilatory restriction in the *AnxA2*$^{-/-}$ mouse lung.

Abnormal epithelial cell morphology in the *AnxA2*$^{-/-}$ mouse lung

Hematoxylin and eosin staining of *AnxA2*$^{+/+}$ and *AnxA2*$^{-/-}$ lung tissue from resting mice showed normal cellularity and arborization of bronchioles and alveoli. However, cross-sections through terminal bronchioles, as well as sections at other levels of airway ramification, revealed increased basophilia and dense, flattened bronchiolar epithelial cells (BECs) (Fig. 2A,B). At the same time, basement membrane autofluorescence, which is imparted by collagens and elastin (Evans et al., 2000), was indistinct in *AnxA2*$^{-/-}$ lung tissue (Fig. 2C,D). Examination of Toluidine-Blue-stained 1 µm sections revealed the absence of a discrete, compact basement membrane, lack of apical Clara cell (or non-ciliated bronchiolar secretory cell) protrusions and a paucity of cilia in *AnxA2*$^{-/-}$ BECs (Fig. 2E,F). Electron microscopy further demonstrated the indistinct nature of the *AnxA2*$^{-/-}$ bronchiolar basement membrane (supplementary material Fig. S1B,C). Scoring of cells lining bronchioles 65–85 µm in diameter confirmed a reduction in the proportion of ciliated cells within *AnxA2*$^{-/-}$ bronchioles (8.3±0.34%, mean ± s.e.; $n=6$) compared with *AnxA2*$^{+/+}$ bronchioles (47.5±3.7, $n=8$; $P<0.001$) (Fig. 2G). These data suggest abnormalities in both bronchiolar epithelial cells and their basement membranes.

Altered COL6 distribution in *AnxA2*$^{-/-}$ bronchiolar basement membranes

Immunostaining of bronchioles from *AnxA2*$^{+/+}$ and *AnxA2*$^{-/-}$ mice confirmed that ANXA2 was localized mainly within the basal portions of bronchial epithelial cells, in close proximity to the autofluorescent basement membrane (Vishwanatha et al., 1995) (Fig. 2H). To determine the expression level and distribution of bronchiolar basement membrane proteins in the *AnxA2*$^{-/-}$ lung, a hierarchical approach was adopted (supplementary material Table S1). From a database of mouse lung matrix proteins, we selected those for which basement membrane-specific expression had been demonstrated (16 proteins), for which staining antibodies were available (11 proteins), and for which expression in the adult mouse lung had been documented (7 proteins) (Manabe et al., 2008). We then compared the expression pattern of these seven proteins (tropoelastin, keratin 5, collagen I, collagen IV, laminin A, fibrillin-1 and COL6) in lung tissue from resting *AnxA2*$^{+/+}$ versus *AnxA2*$^{-/-}$ (supplementary material Fig. S2; Fig. 3A–C). Although six proteins showed no difference in staining pattern (supplementary material Fig. S2), basement membrane staining for COL6 was indistinct in the *AnxA2*$^{-/-}$ lung and mirrored the loss of basement-membrane-associated autofluorescence. Upon quantification of staining intensity over a series of stained sections, we noted that peribronchiolar basement membrane staining of COL6 in *AnxA2*$^{+/+}$ was, on average, 3.3-times greater than that of *AnxA2*$^{-/-}$ tissue (18.4±2.4 versus 5.6±1.6 arbitrary units; mean ± s.e., $n=6$, $P<0.01$) (Fig. 3A–C). These data suggest a COL6-specific defect in synthesis, processing or secretion in *AnxA2*$^{-/-}$ bronchial epithelial cells.

Lung stiffness in the *Col6a1*$^{-/-}$ mouse phenocopies the *AnxA2*$^{-/-}$ mouse

Evaluation of pulmonary biomechanics in *Col6a1*$^{-/-}$ versus *Col6a1*$^{+/-}$ mice revealed a profile very similar to that observed in the *AnxA2*$^{-/-}$ mouse. Dynamic, but not static, compliance was significantly decreased (Fig. 3D,E; $P<0.0001$ and $P=0.578$, respectively), whereas both whole lung and tissue elastance were correspondingly increased (Fig. 3F,G; $P=0.0076$ and $P<0.0001$, respectively). As in the *AnxA2*$^{-/-}$ mouse, total dynamic resistance was increased in the *Col6a1*$^{-/-}$ lung (Fig. 3H; $P<0.0001$), but airway resistance showed no significant change (Fig. 3I; $P=0.276$). Tissue dampening was also increased (Fig. 3J; $P<0.0001$), whereas inspiratory capacity was not significantly affected (Fig. 3K; $P=0.0639$). Because *Col6a1*$^{-/-}$ mice lack immunodetectable triple helical COL6 (Bonaldo et al., 1998), these data indicate that loss of mature COL6 leads to a significant reduction in dynamic compliance and an increase in hyperelastic recoil, thus providing a potential explanation for the pulmonary dysfunction in the *AnxA2*$^{-/-}$ mouse.

COL6 is retained within a trypsin-protected microsomal compartment in *AnxaA2*$^{-/-}$ cells

In evaluating nonciliated BECs in lung tissue from resting mice, electron-dense secretory granules were almost twice as abundant in *AnxA2*$^{-/-}$ BECs compared with *AnxA2*$^{+/+}$ BECs (Fig. 4A). To determine the potential role of ANXA2 in secretion of COL6, we stained *AnxA2*$^{+/+}$ and *AnxA2*$^{-/-}$ primary mouse embryonic fibroblasts (mEFs) at 90% confluence with antibody directed against COL6 (Fig. 4B). Immunoreactive material was identified within 200–1000 nm punctate structures that were, on average, 4-times more abundant in *AnxA2*$^{-/-}$ than *AnxA2*$^{+/+}$ cells (62.7±2.9 vs 16.5±3.2, mean ± s.e., $n=6$–8, $P<0.001$). These data were consistent with the increased abundance of electron-dense secretory granules in *AnxA2*$^{-/-}$ BECs observed by electron microscopy (Fig. 4A).

We assessed steady state synthesis of COL6 in *AnxaA2*$^{+/+}$ and *AnxaA2*$^{-/-}$ lung tissue. Semi-quantitative and quantitative real-time RT-PCR analyses of *Col6a1*, *Col6a2* and *Col6a3* transcripts, which encode the COL6 alpha1, alpha2 and alpha3 isoforms, respectively, revealed no significant differences in transcript levels (Fig. 4C). However, immunoblots of reduced whole-lung homogenates revealed that total protein levels of COL6a1 and COL6a2 were diminished in *AnxA2*$^{-/-}$ lungs (Fig. 4D). Interestingly, no difference in the abundance of protomeric, intracellular COL6, which is soluble in Triton X-100 (Engvall et al., 1986), was detected, whereas highly crosslinked extracellular COL6, which is insoluble in Triton X-100 (Engvall et al., 1986), was markedly reduced in *AnxA2*$^{-/-}$ compared with *AnxA2*$^{+/+}$ tissues (Fig. 4E). Based on these data, we concluded that the reduction in total COL6 protein in *AnxA2*$^{-/-}$ lung tissue reflected a defect in its post-transcriptional processing, deposition or stability within the basement membrane.

To identify the location of COL6 within *AnxA2*$^{-/-}$ cells, we probed subcellular microsomal and cytosolic fractions by immunoblotting. In *AnxA2*$^{+/+}$ lung homogenate, ANXA2 was present, as expected, in both compartments (Fig. 4F). However, although some COL6 was present in *AnxA2*$^{-/-}$ cytosol, it was highly enriched in *AnxA2*$^{-/-}$, but not *AnxA2*$^{+/+}$, microsomes. Blotting for calnexin (CNX), a microsomal marker, and lactate

Journal of Cell Science (2014) 127, 828–844 doi:10.1242/jcs.137802

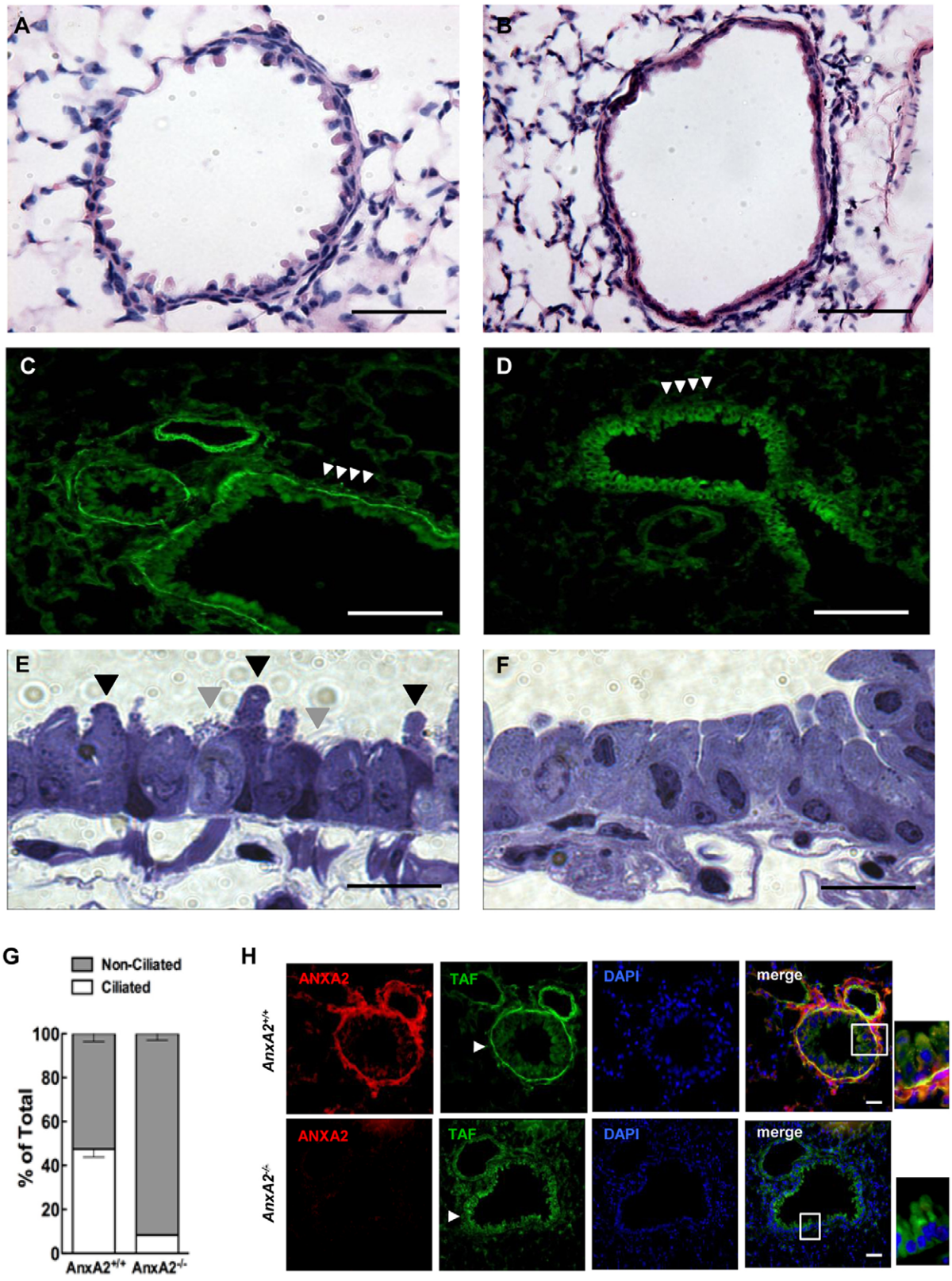

Fig. 2. Aberrant bronchial epithelial morphology and abnormal distribution of extracellular matrix proteins in the AnxA2-deficient mouse lung. (A,B) Hematoxylin and eosin staining in *AnxA2*$^{+/+}$ (A) and *AnxA2*$^{-/-}$ (B) bronchioles. (C,D) Tissue autofluorescence (TAF, green) in *AnxA2*$^{+/+}$ (C) and *AnxA2*$^{-/-}$ (D) bronchioles captured using a FITC fluorescence filter with UV excitation (green; white arrowheads indicate basement membrane). (E,F) Toluidine-Blue-stained thin sections of *AnxA2*$^{+/+}$ (E) and *AnxA2*$^{-/-}$ (F) bronchiolar epithelium; black and gray arrowheads indicate Clara and ciliated cells, respectively. (G) Differential counts of ciliated and non-ciliated epithelial cells in *AnxA2*$^{+/+}$ and *AnxA2*$^{-/-}$ bronchioles (means ± s.e., n=6–8; P<0.001). (H) Frozen sections of lung tissue imaged for TAF (green), ANXA2 (red) and DAPI (blue). Insets show magnified views of boxed areas. Arrowheads indicate basement membrane. Scale bars: 50 μm (A–D), 10 μm (E,F), 40 μm (H).

Journal of Cell Science

Journal of Cell Science (2014) 127, 828–844 doi:10.1242/jcs.137802

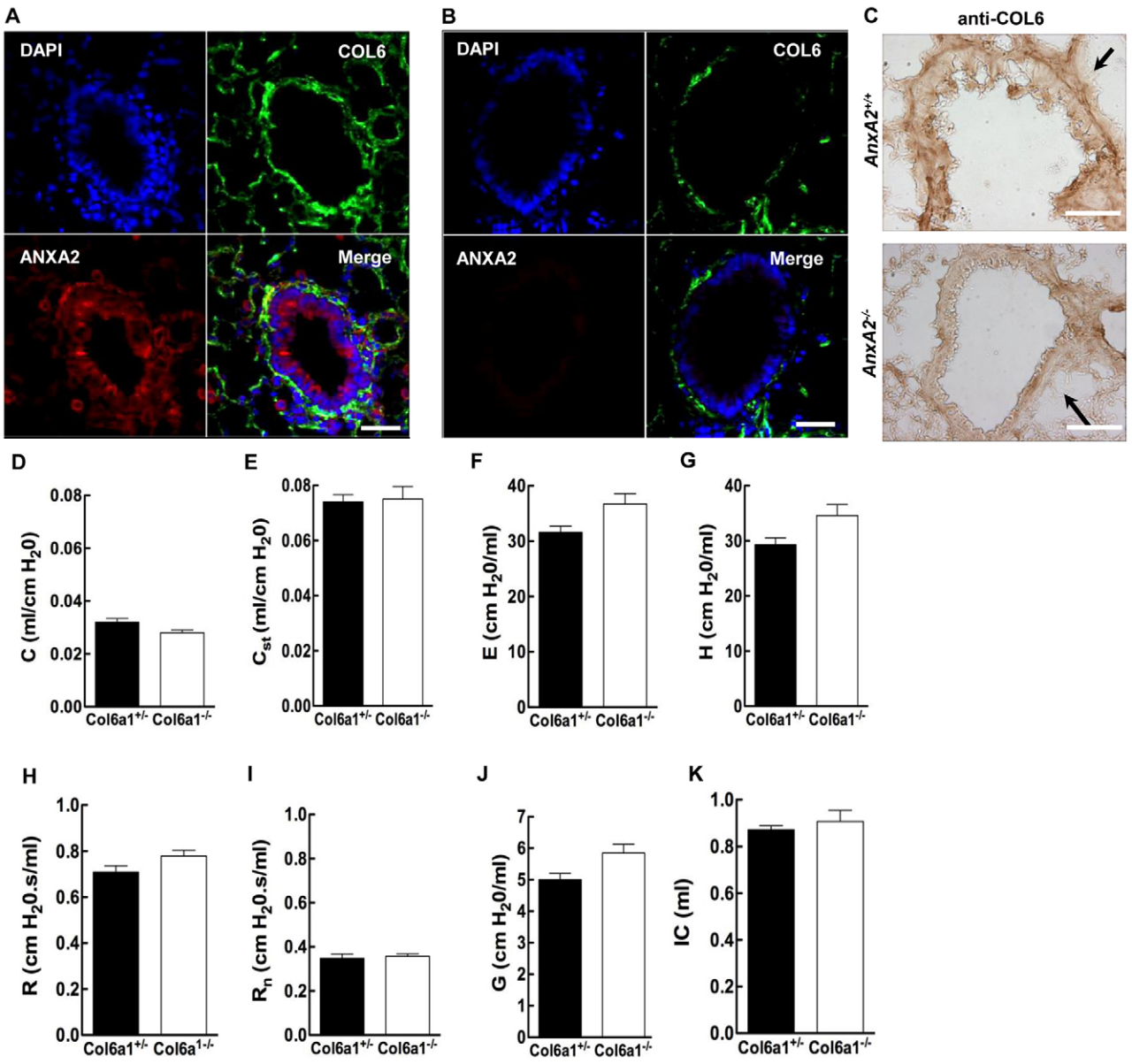

Fig. 3. COL6 is deficient in *AnxA2*$^{-/-}$ bronchiolar epithelial basement membranes and COL6 deficiency is associated with a restrictive ventilatory defect. (A) Frozen sections from *AnxA2*$^{+/+}$ (A) and *AnxA2*$^{-/-}$ (B) mouse lung tissue stained for ANXA2 (red), COL6 (green) and nuclei (DAPI, blue). (C) Mouse lung tissue from *AnxA2*$^{+/+}$ and *AnxA2*$^{-/-}$ mice was incubated with anti-COL6 IgG and then labeled with DAB. Arrows indicate basement membrane. (D–K) Lung biomechanics in *Col6a1*$^{+/-}$ and *Col6a1*$^{-/-}$ mice. Shown are dynamic (D) and static (E) compliance, whole-lung (F) and tissue (G) elastance, total dynamic (H) and airway (I) resistance, tissue dampening (J) and inspiratory capacity (K). Data represent means ± s.e. $P<0.0001$ for all genotype pairs, except for static compliance (E; $P=0.578$), whole-lung elastance (F; $P=0.0076$), airway resistance (I; $P=0.276$) and inspiratory capacity (K; $P=0.0639$). $n=9$ for all groups. Scale bars: 50 μm.

dehydrogenase (LDH), a cytosolic marker, demonstrated complete separation of the two fractions. To investigate whether microsome-associated COL6 and ANXA2 occupied intra- or extravesicular compartments, we next subjected microsomes from lung homogenates to limited proteolysis using a trypsin-protection assay (Fig. 4G). Whereas full-length, native COL6 is sensitive to tryptic digestion (not shown), microsomal COL6 was not affected by tryptic hydrolysis. However, microsome-associated ANXA2 disappeared almost completely within 60 minutes. From these data, we conclude that COL6 accumulates within a trypsin-protected, microsomal environment, whereas ANXA2 occupies an unprotected, but neighboring location.

ANXA2 and COL6 closely associate on electron-dense granules in nonciliated secretory bronchiolar epithelial cells

To address the potential physical association between ANXA2 and COL6, we conducted immunoprecipitation assays. Anti-COL6 IgG, but not isotype-matched control IgG, precipitated both COL6 and ANXA2 from whole *AnxA2*$^{+/+}$ lung extracts, and COL6 from whole *AnxA2*$^{-/-}$ lung extracts (Fig. 5A). Similarly, anti-ANXA2 IgG immunoprecipitated both ANXA2 and COL6 from whole

Journal of Cell Science (2014) 127, 828–844 doi:10.1242/jcs.137802

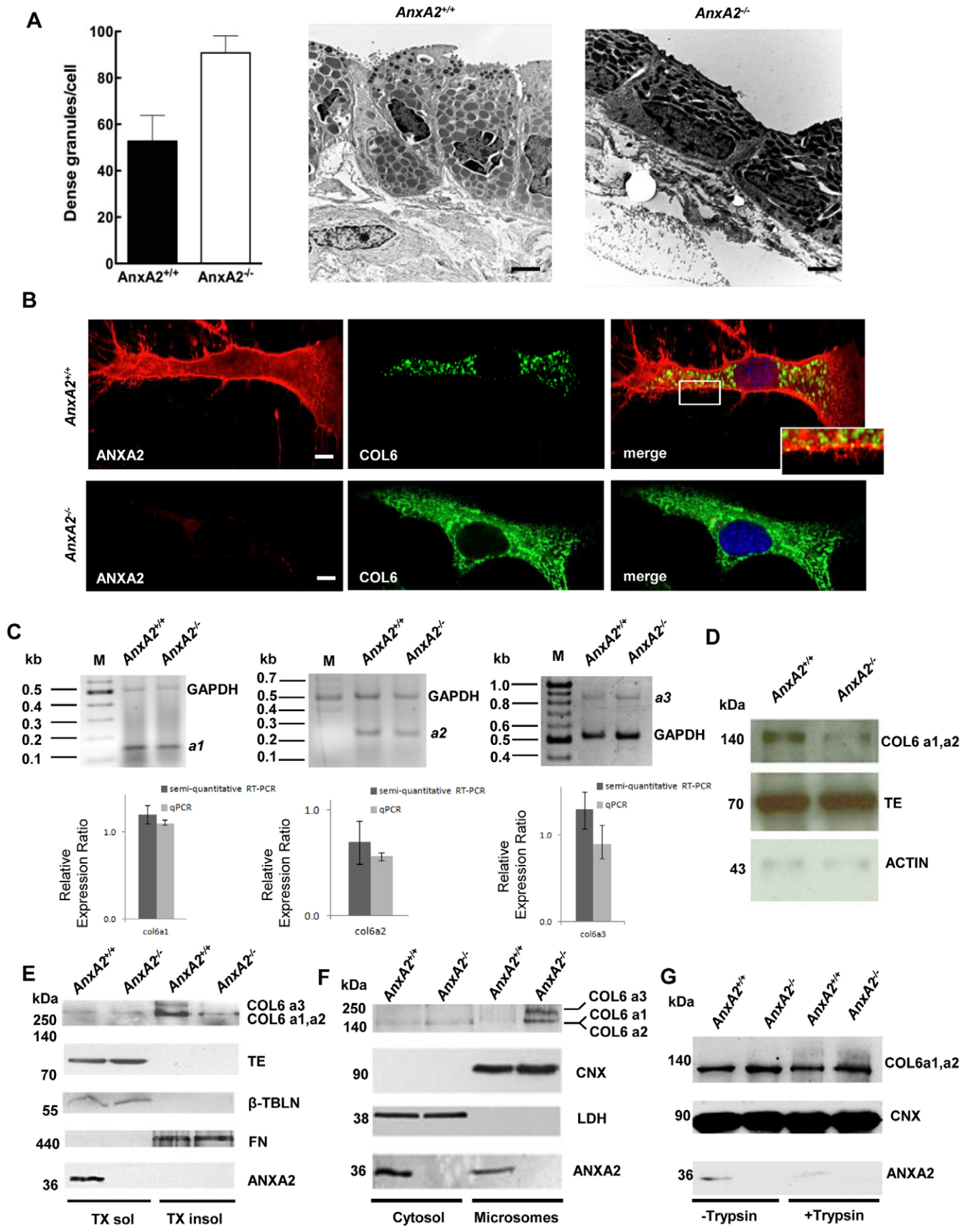

Fig. 4. See next page for legend.

Journal of Cell Science

Journal of Cell Science (2014) 127, 828–844 doi:10.1242/jcs.137802

Fig. 4. COL6 is associated with electron-dense granules and retained within microsomes in *AnxAa2*$^{-/-}$ BECs. (A) Number of dense granules in *AnxA2*$^{+/+}$ (left) and *AnxAa2*$^{-/-}$ (right) BECs (means ± s.e., n=9–11 cells; P<0.001). (B) mEFs were co-stained for ANXA2 (red), COL6 (green) and nuclei (DAPI, blue). Inset shows magnified view of boxed area. (C) Semi-quantitative RT-PCR for COL6a1 (139 bp), COL6a2 (241 bp) and COL6a3 (865 bp) transcripts in *AnxA2*$^{+/+}$ and *AnxA2*$^{-/-}$ genotypes (top). Relative expression ratios for COL6 genes obtained by semi-quantitative RT-PCR (dark bars) were compared with those obtained by qPCR (light bars) (bottom). GAPDH (530 bp) served as an internal control for normalization (means ± s.e., n=3 replicates). (D) COL6 from whole-lung homogenates was analyzed by immunoblot under reducing conditions. Actin and tropoelastin (TE) represent loading controls. (E) Immunoblot of COL6 in Triton-X-100-soluble and -insoluble whole-lung fractions. β-tubulin (β-TBLN) and tropoelastin (TE) represent loading controls for soluble fractions and fibronectin (FN) for insoluble fractions. (F) COL6 in cytosolic and microsomal fractions. Calnexin (CNX) and lactate dehydrogenase (LDH) represent loading controls and markers for microsomal and cytosolic fractions, respectively. (G) Immunoblot of microsomes, isolated as in F, and subjected to limited tryptic digestion. CNX is the loading control. Scale bars: 5 μm (A), 25 μm (B).

AnxA2$^{+/+}$, but neither protein from *AnxA2*$^{-/-}$ lung extracts (Fig. 5B). These results suggest that ANXA2 and COL6 undergo a physical association that could be either direct or indirect.

To further evaluate the physical proximity between ANXA2 and COL6 within the bronchiolar epithelial cell *in vivo*, we conducted immunoelectron microscopy studies. In BECs from lung tissue of resting mice, anti-ANXA2- and anti-COL6-conjugated immunogold beads (10 nm and 6 nm diameter, respectively) co-associated in clusters located at the membrane borders of large, intracellular vesicles enclosing electron dense material (Fig. 5C). Parallel analyses in *AnxA2*$^{-/-}$ BECs revealed the absence of anti-ANXA2-labeled beads, and a reduction in the total number of clustered anti-COL6-conjugated beads. Within *AnxA2*$^{+/+}$ bronchial epithelial cells, we found an average of six COL6 beads per ANXA2–COL6 cluster, whereas clusters in *AnxA2*$^{-/-}$ BECs contained an average of only two 6 nm beads (Fig. 5D). In addition, whereas 71% of COL6 beads in *AnxA2*$^{+/+}$ BECs were associated with membrane-bound, secretory vesicle-like structures, only 31% were vesicle associated in *AnxA2*$^{-/-}$ BECs (Fig. 5E). These data also suggest a physical association between ANXA2 and COL6 within secretory vesicles.

ANXA2 modulates COL6 secretion by mEFs

To analyze COL6 secretion in the presence and absence of ANXA2, we transduced primary *AnxA2*$^{-/-}$ mEFs with adenoviral constructs encoding either GFP alone (AdV-null) or a GFP–ANXA2 fusion construct (AdV-A2) (Fig. 5F). At 72 hours, immunoblot analysis revealed that COL6 was expressed within *AnxA2*$^{+/+}$ and *AnxA2*$^{-/-}$ cells, regardless of viral transduction (Fig. 5F, left panel). COL6 was also detected in matrix secreted by *AnxA2*$^{+/+}$ cells or *AnxA2*$^{-/-}$ cells transduced with AdV-A2, but not in matrix produced by *AnxA2*$^{-/-}$ cells or *AnxA2*$^{-/-}$ cells transduced with AdV-null. In the matrix, there was, on average, 7-times more COL6 in *AnxA2*$^{-/-}$ AdV.rA2 samples compared with *AnxA2*$^{-/-}$ samples, and 14-times more COL6 compared with *AnxA2*$^{-/-}$ AdV-null samples (4.2±0.9 versus 0.6±0.3 and 4.2±0.9 versus 0.3±0.1 arbitrary units, respectively, mean ± s.e., n=3, P<0.05). There was no significant difference between COL6 in *AnxA2*$^{-/-}$ AdV.rA2 samples, compared with *AnxA2*$^{+/+}$ samples (P>0.1) (Fig. 5F, right panel). Similarly, primary *AnxA2*$^{+/+}$ mEFs transduced with a GFP–COL6 fusion construct secreted GFP into the extracellular space, where it was detected by Rhodamine-conjugated anti-GFP following fixation under nonpermeabilizing conditions (Fig. 5G, top panel). By contrast, extracellular GFP tag was not detected in association with *AnxA2*$^{-/-}$ mEFs transfected with the same construct (Fig. 5G, bottom panel). Cells transduced with a construct encoding GFP alone did not release GFP into the extracellular milieu (not shown). Together, these data demonstrate that expression of ANXA2 is required for efficient secretion of COL6 by primary mEFs.

Both ANXA2 and COL6 interact with SNARE complex proteins in bronchiolar epithelial cells

In cultured neuroendocrine and type II alveolar pneumocytes, ANXA2 has been reported to interact with members of the SNARE family of membrane fusion proteins (Umbrecht-Jenck et al., 2010; Wang et al., 2007). In pull-down assays in *AnxA2*$^{+/+}$ whole-lung extracts, similarly, we found that anti-COL6 IgG specifically precipitated ANXA2, as well as SNAP-23, VAMP2 and syntaxin 2 (Fig. 6A). In parallel samples from *AnxA2*$^{-/-}$ lung extracts, anti-COL6 precipitated SNAP-23, VAMP2 and syntaxin 2, indicating that the association between COL6, SNAP-23, VAMP2 and syntaxin2 was independent of ANXA2. Immunoelectron microscopy studies, furthermore, revealed that ANXA2 specifically colocalized with both SNAP-23 and VAMP2 in BECs from *AnxA2*$^{+/+}$ lungs, whereas fewer SNAP-23 and VAMP2-related beads (52±1%, n=10 versus 14±1%, n=16; means ± s.e.) were associated with secretory-vesicle-like structures in *AnxA2*$^{-/-}$ BECs (Fig. 6B). Together, these data demonstrate that ANXA2 associates with SNARE complexes, thereby enabling secretion of COL6.

Absence of ANXA2 arrests COL6 in a late-Golgi VAMP2-positive compartment

We used standard markers for specific intracellular compartments to analyze the location of COL6 at multiple points along the secretory pathway in *AnxA2*$^{+/+}$ and *AnxA2*$^{-/-}$ mouse embryonic fibroblasts (mEFs) (Fig. 6C and supplementary material Fig. S3C,D). We found no colocalization of anti-COL6 immunoreactive material and MitoTracker in either *AnxA2*$^{+/+}$and *AnxA2*$^{-/-}$ mEFs (supplementary material Fig. S3C). In addition, we found slight colocalization of anti-COL6 immunoreactivity with the endoplasmic reticulum (ER) marker GRP94, but this did not differ between *AnxA2*$^{+/+}$ and *AnxA2*$^{-/-}$ mEFs (Fig. 6C). Similar results were obtained upon staining for a second ER marker, anti-calnexin (supplementary material Fig. S3D). However, staining for the trans-Golgi marker (TGN38) revealed significant colocalization with anti-Col6 reactivity within *AnxA2*$^{-/-}$ cells, but only minimal colocalization in *AnxA2*$^{+/+}$ cells (Fig. 6C). Finally, staining for VAMP2, generally considered to reside within post-Golgi secretion compartments, colocalized with anti-COL6 in a manner that was much more prominent in *AnxA2*$^{-/-}$ than in *AnxA2*$^{+/+}$ mEFs. At the same time, immunoelectron microscopy of BECs *in situ* showed COL6 to be present in VAMP2-positive electron-dense structures in *AnxA2*$^{+/+}$, but not *AnxA2*$^{-/-}$, cells (supplementary material Fig. S4A,B). Together, these data indicate that COL6 is retained within a late-Golgi VAMP2-positive compartment.

Knockdown of SNARE proteins arrests COL6 within a late-Golgi VAMP2-positive compartment

By immunofluorescence microscopy, siRNA knockdown of SNAREs known to interact with ANXA2 led to accumulation of

Journal of Cell Science (2014) 127, 828–844 doi:10.1242/jcs.137802

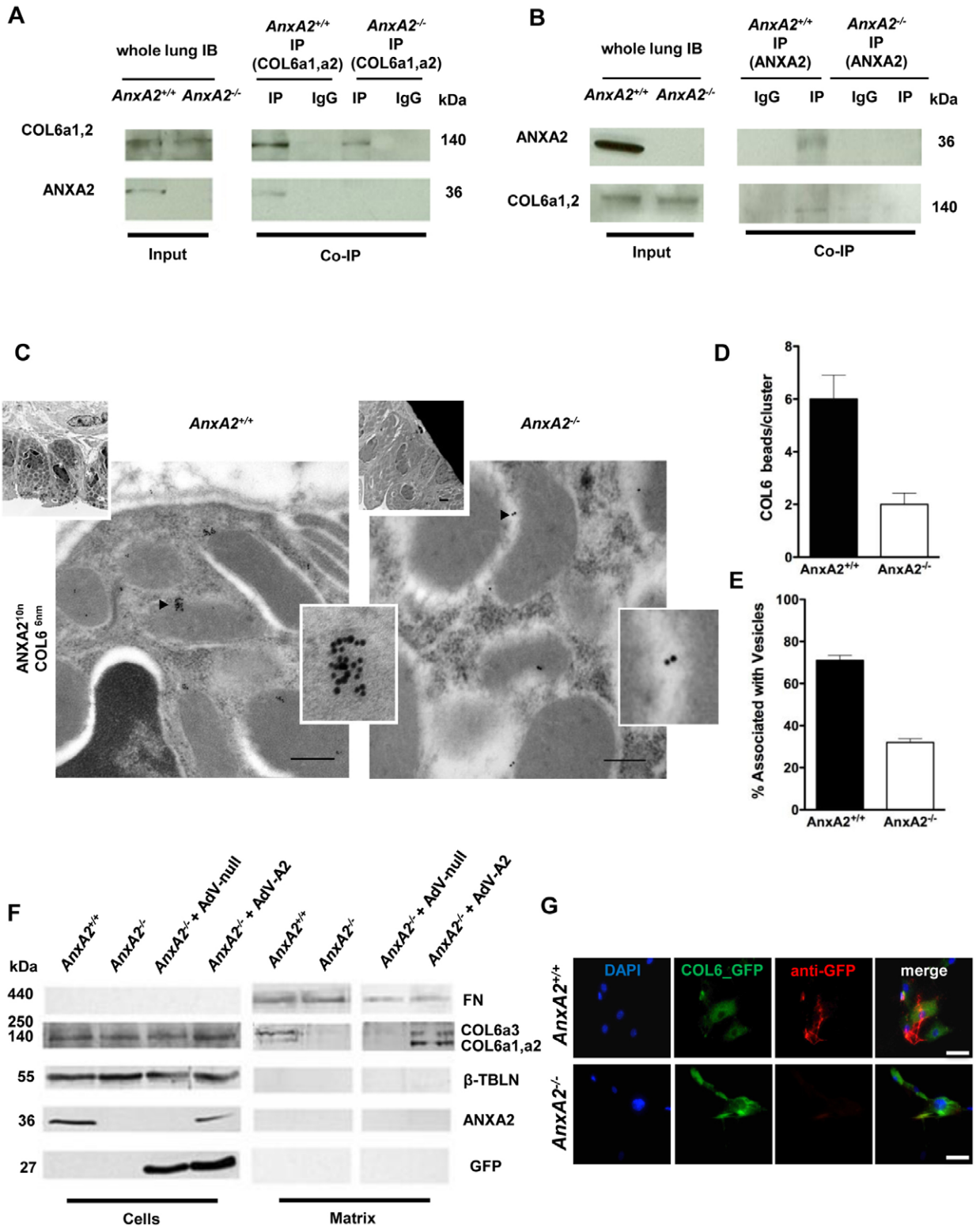

Fig. 5. ANXA2 interacts with COL6 and mediates COL6 secretion. (A) Anti-COL6a1 and COL6a2 immunoprecipitates (IPs) from whole-lung lysate extracts were immunoblotted for COL6a1, a2 and ANXA2. (B) Reciprocal anti-ANXA2 IPs were immunoblotted for ANXA2 and COL6a1, a2. Non-immune IgG served as the IP control. (C) Colocalization of ANXA2 (10 nm gold particle) and COL6 (6 nm) in *AnxA2*$^{+/+}$ and *AnxA2*$^{-/-}$ BECs. Arrowheads indicate areas expanded in insets. (D) Number of COL6-related beads per cluster in *AnxA2*$^{+/+}$ and *AnxA2*$^{-/-}$ BECs (means ± s.e., n=8, P=0.038). (E) Proportion of beads (both ANXA2 and COL6) associated with dense-core granules (means ± s.e., n=8, P=0.00008). (F) Cell lysates and matrix extracts from mEFs transduced with GFP-encoding AdV-null or AdV-A2 vectors analyzed by immunoblot under reducing conditions. GFP expression served as an index of cell infection. β-TBLN indicates the cell fraction and FN, the matrix. (G) mEFs were transfected with a COL6A1–GFP fusion construct and fixed at 48 hours with 2% PFA. Secreted COL6 was labeled with anti-GFP (red). Intrinsic GFP fluorescence was quenched with 50 mM NH_4Cl. Merged images show intracellular (green) versus extracellular (red) distribution of COL6. Scale bars: 200 nm (C), 75 μm (G).

Journal of Cell Science (2014) 127, 828–844 doi:10.1242/jcs.137802

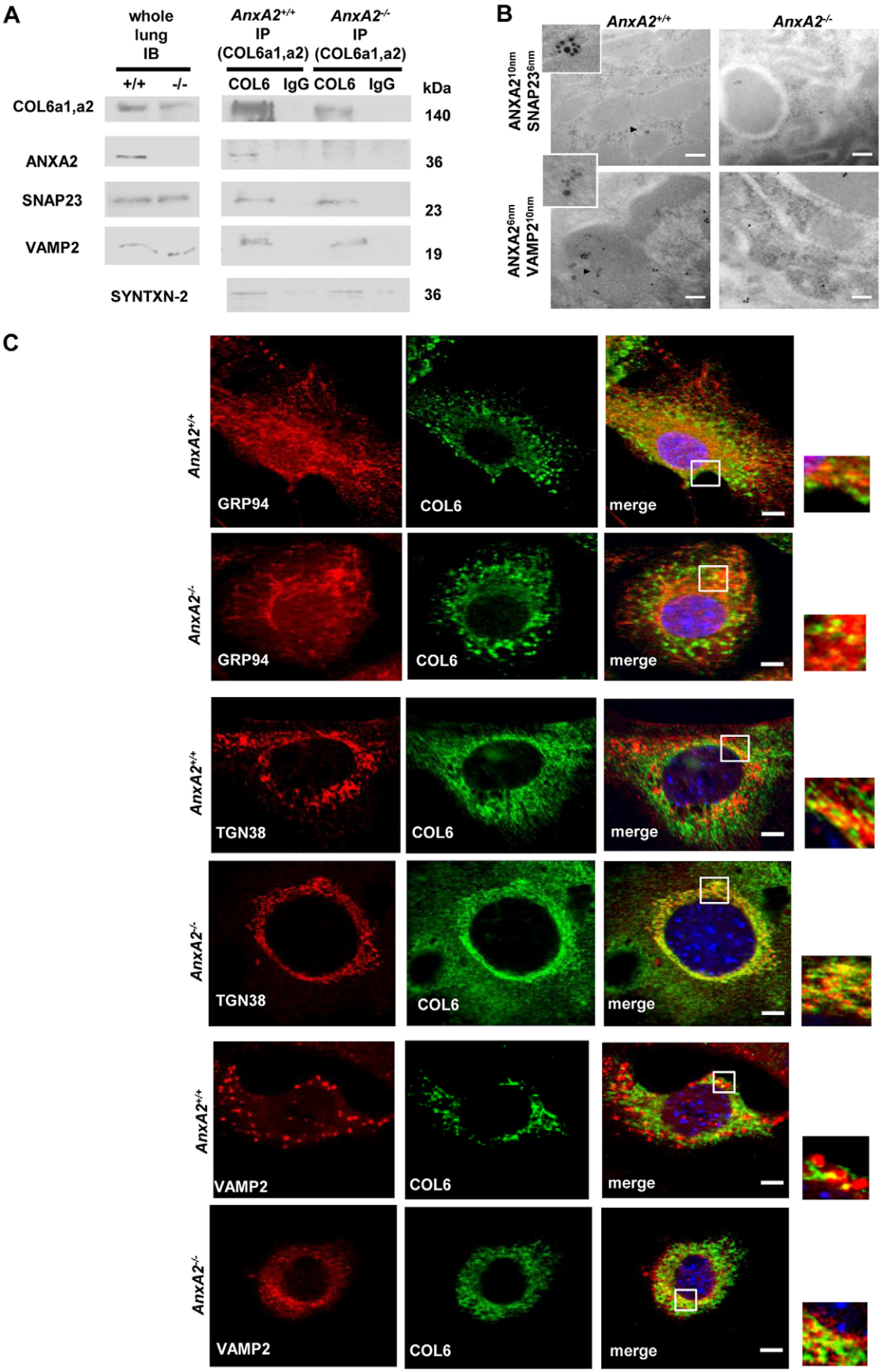

Fig. 6. ANXA2 interacts with SNAREs and enables release of COL6 from a late-Golgi VAMP2-positive compartment. (A) Anti-COL6a1,a2 immunoprecipitates from whole-lung lysates were immunoblotted with antibodies directed against COL6a1,a2, ANXA2, SNAP-23, VAMP2 and syntaxin-2. (B) Immunogold labeling. Top panels, SNAP-23 (6 nm gold particles) and ANXA2 (10 nm gold particles). Bottom panels, VAMP2 (10 nm gold particles) and ANXA2 (6 nm). Arrowheads indicate areas expanded in insets. (C) mEFs stained with standard markers for specific intracellular compartments, including GRP94 (ER), TGN38 (trans-Golgi) and MitoTracker and CNX (ER) (supplementary material Fig. S3C, S3D), as well as VAMP2. Scale bars: 200 nm (B), 10 μm (C).

Journal of Cell Science (2014) 127, 828–844 doi:10.1242/jcs.137802

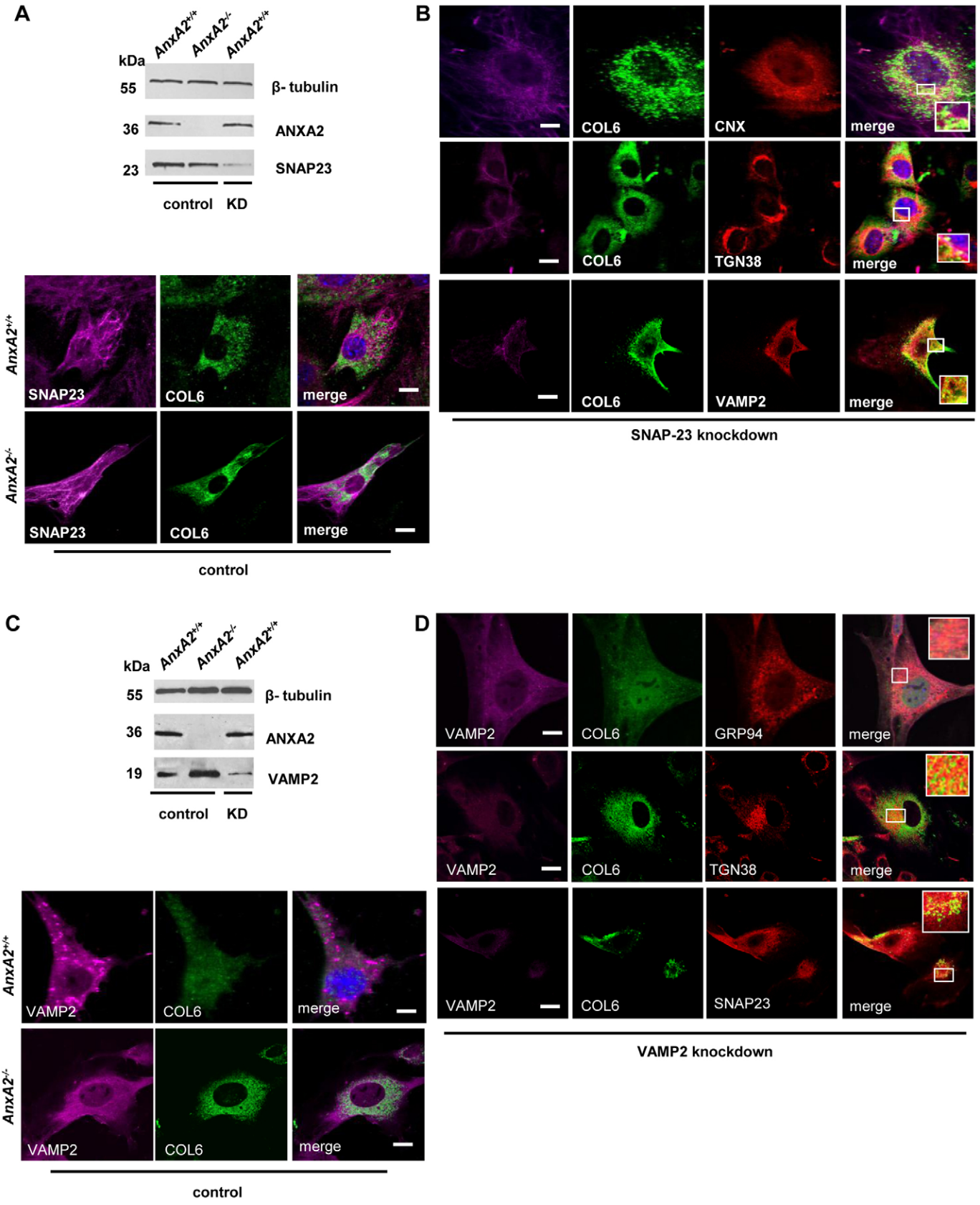

Fig. 7. See next page for legend.

Journal of Cell Science (2014) 127, 828–844 doi:10.1242/jcs.137802

Fig. 7. Knockdown of SNARE proteins arrests COL6 in a late-Golgi VAMP2-positive compartment. (A) Lysates from mEFs transfected with control and SNAP-23 siRNA were analyzed by immunoblotting. β-tubulin served as a loading control (top). mEFs transfected with mock siRNA were stained for SNAP-23, COL6 and nuclei (DAPI, blue) (bottom). (B) mEFs transfected with SNAP-23 siRNA were stained for COL6 and CNX (ER), TGN38 (trans-Golgi) or VAMP2 with DAPI. (C) Lysates from mEFs transfected with control and VAMP2 siRNA analyzed as in A. mEFs transfected with mock siRNA were stained for VAMP2, COL6 and DAPI (bottom). (D) mEFs transfected with VAMP2 siRNA were stained for COL6 and GRP94 (ER), TGN38 (trans-Golgi) or SNAP-23 and DAPI. Scale bars: 20 μm.

intracellular COL6 (Fig. 7). Specifically, and as seen in *AnxA2*$^{-/-}$ cells, we found increased association of anti-COL6 and anti-TGN38 immunoreactivity in cells depleted of either SNAP-23 (Fig. 7A,B) or VAMP2 (Fig. 7C,D). These data indicate that both SNAP-23 and VAMP2 play a functional role in the secretion of COL6.

Loss of ANXA2 results in BEC dropout, apoptosis and secretion defects

We observed abnormalities in both BECs and their basement membranes, in association with a reduced proportion of ciliated cells in the *AnxA2*$^{-/-}$ mouse (Fig. 2A–G). To determine whether an alteration in the bronchiolar basement membrane compromises epithelial cell adhesion and/or survival in the *AnxA2*$^{-/-}$ mouse, we carried out bronchoalveolar lavage (BAL) (Fig. 8A). BAL fluid from *AnxA2*$^{+/+}$ and *AnxA2*$^{-/-}$ mice contained equivalent concentrations of cells (152±14 vs 158±14 cells/μl, respectively; mean ± s.e., $n=6$) with similar total volumes of BAL fluid retrieved. Differential cell counts, however, revealed an excess of epithelial cells in fluid recovered from *AnxA2*$^{-/-}$ mice (34±12 vs 10±4%, $n=6$, $P=0.001$), and a corresponding reduction in macrophages (62±10 vs 87±3%, $n=6$, $P=0.0002$). This result suggested a higher rate of bronchial epithelial cell disadhesion in response to the lavage procedure.

Loss of cell–matrix adhesion might induce epithelial cell apoptosis (anoikis) (Frisch and Screaton, 2001; Taddei et al., 2012). We, therefore, conducted TUNEL staining of lung sections, which revealed dramatically increased nucleic acid breakage within bronchial epithelial cells of *AnxA2*$^{-/-}$ compared with *AnxA2*$^{+/+}$ lungs (Fig. 8B). Further staining revealed that *AnxA2*$^{-/-}$ bronchiolar epithelial cells contained twice as many activated caspase-3-positive epithelial cells than *AnxA2*$^{+/+}$ bronchioles, confirming an increased rate of apoptosis (Fig. 8C,D).

To determine whether the secretion-enabling role of ANXA2 is unique to the bronchial epithelial cell or seen in other tissues, we examined skeletal muscle from *AnxA2*$^{+/+}$ and *AnxA2*$^{-/-}$ mice (Fig. 8E). In this tissue, interstitial fibroblasts are the main source of COL6 (Bönnemann 2011; Zou et al., 2008). Interestingly, immunofluorescence staining revealed an accumulation of COL6 between individual myofibers cut in cross-section, the precise location where interstitial fibroblasts are located. This finding is consistent with our studies on mEFs, which also accumulated and failed to secrete COL6 (Fig. 4B and Fig. 5F,G). These data suggest that ANXA2-mediated secretion of COL6 is not limited to the bronchial epithelial cell, but also occurs in tissue fibroblasts.

COL6 rescues defective cell–matrix adhesion in ANXA2-deficient cells

To determine whether cell adhesion to extracellular matrix and basement membrane might be COL6-dependent, we conducted a series of cell-adhesion assays using (Fig. 8F). Whereas 60–70% of cells of both genotypes adhered well to matrices produced by *AnxA2*$^{+/+}$ mEFs, only 20–30% of each genotype adhered to matrices produced by *AnxA2*$^{-/-}$ mEFs. In addition, *AnxA2*$^{+/+}$ mEFs were superior to *AnxA2*$^{-/-}$ mEFs in adhering to uncoated or BSA-coated polystyrene. Interestingly, however, supplementation of COL6 completely corrected the defect in *AnxA2*$^{-/-}$ mEF adhesion to BSA. These data indicate that COL6 supports cell adhesion to extracellular matrix substrates, and suggest that the reduced matrix adhesion displayed by *AnxA2*$^{-/-}$ bronchial epithelial cells is associated with a deficiency of COL6.

DISCUSSION

These data reveal for the first time that deficiency of ANXA2 results in aberrant secretion of COL6, but not other collagens, from bronchial epithelial cells into basement membranes. Failure to secrete COL6 is associated with attenuated cell–matrix adhesion, apoptosis and physiologically significant pulmonary stiffness with reduced exercise tolerance. In the *AnxA2*$^{-/-}$ lung, histological studies revealed bronchial epithelial cell dysmorphology and apoptosis, together with an altered basement membrane that lacked COL6. Despite equivalent mRNA levels for COL6 in *AnxA2*$^{-/-}$ and *AnxA2*$^{+/+}$ lung tissue, we found diminished overall COL6 protein levels, reduced matrix-associated COL6 and retention of COL6 within a trypsin-protected, microsomal fraction in *AnxA2*$^{-/-}$ lung cells. In cultured *AnxA2*$^{-/-}$ fibroblasts, moreover, we uncovered a block to COL6 secretion that could be reversed by restoration of ANXA2 expression. Co-immunoprecipitation and immunoelectron microscopy experiments revealed that ANXA2 and COL6 form a complex with the SNARE proteins SNAP-23, VAMP2 and syntaxin 2, which are all components of the epithelial exocytotic machinery. In the absence of ANXA2, COL6 accumulated in a late-Golgi, VAMP2-positive compartment, strongly suggesting impaired fusion of secretory vesicles with the plasma membrane. We found a similar accumulation of COL6 in cells in which either SNAP-23 or VAMP2 had been depleted. Together, these data indicate that ANXA2 promotes bronchial epithelial cell survival and normal biomechanics in the mouse lung, by mediating a unique secretion pathway for macromolecular COL6.

An important question is whether the impairment of COL6 secretion in the *AnxA2*$^{-/-}$ mouse is sufficient to explain the observed respiratory dysfunction and exercise intolerance. Humans with Ullrich congenital muscular dystrophy, which can result from mutations in the *COL6A1*, *COL6A2* or *COL6A3* loci, exhibit a restrictive ventilatory defect that is frequently out of proportion to the degree of myopathy. In a recent study, nearly 50% of still-ambulatory patients suffered from respiratory insufficiency, a distinct difference from Duchenne muscular dystrophy in which respiratory failure typically follows loss of ambulation (Nadeau et al., 2009). Similarly, 16% of patients with Bethlem myopathy, all of whom were still ambulatory, had a forced vital capacity that was less than 70% of the predicted value (van der Kooi et al., 2006). These studies suggest that the earlier development of respiratory insufficiency in disorders due to *COL6* mutations might reflect loss of pulmonary compliance in addition to compromise of muscles of respiration.

In our pulmonary function studies, elastance and compliance were more severely perturbed in *AnxA2*$^{-/-}$ mice compared with *Col6a1*$^{-/-}$ mice. This result suggests that ANXA2 might play a

Journal of Cell Science (2014) 127, 828–844 doi:10.1242/jcs.137802

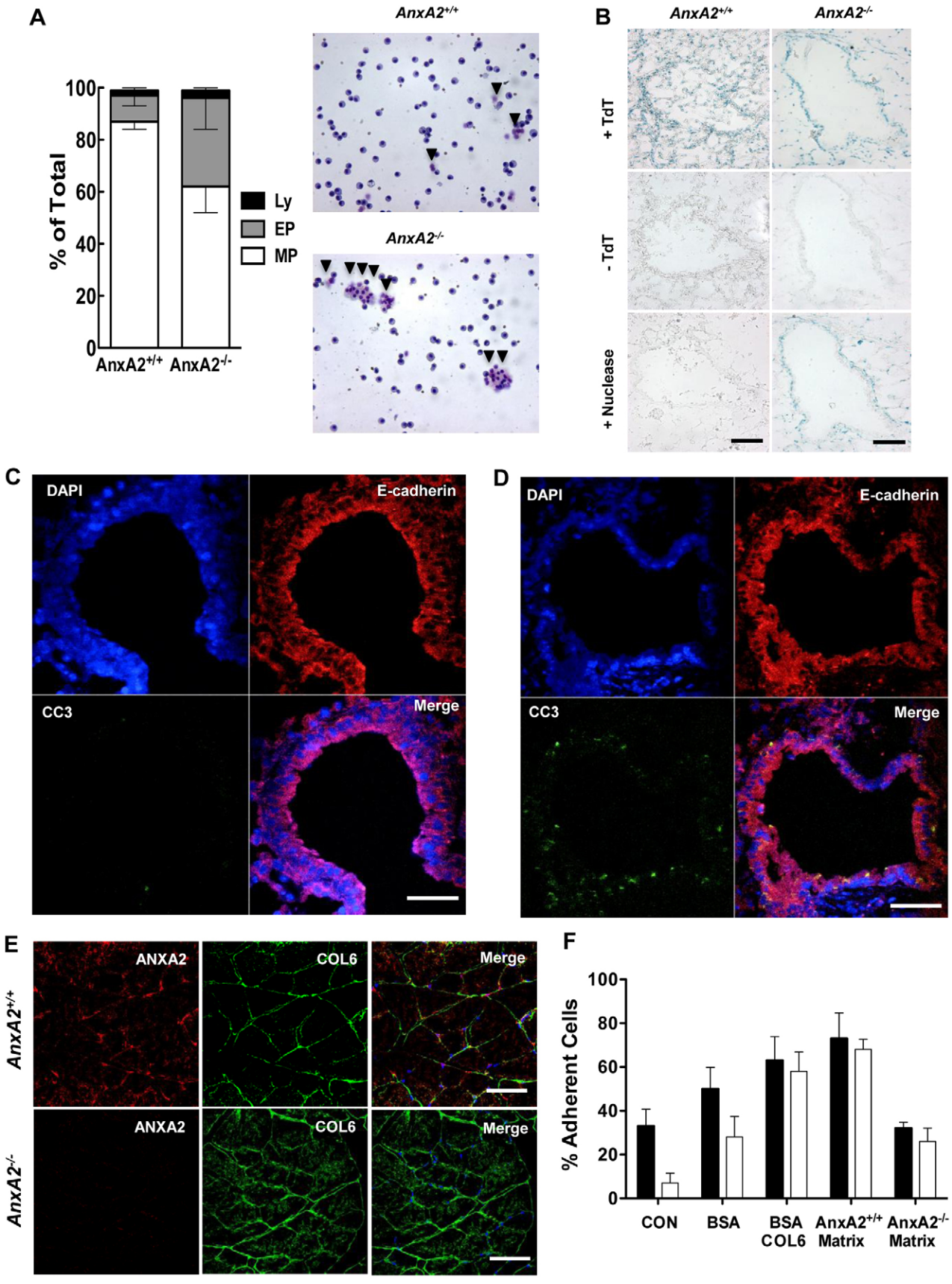

Fig. 8. See next page for legend.

Journal of Cell Science (2014) 127, 828–844 doi:10.1242/jcs.137802

Fig. 8. Absence of ANXA2 is associated with apoptosis, reduced cell adhesion and impaired secretion of COL6 in interstitial skeletal muscle. (A) Total (Trypan Blue) and differential cell counts of lymphocytes (Ly), epithelial cells (EP) and macrophages (MP) in BAL fluid from *AnxA2*$^{+/+}$ (top) and *ANXA2*$^{-/-}$ (bottom) mice. Data represent means ± s.e., n=6) (arrowheads indicate epithelial cells). (B) TUNEL staining of *AnxA2*$^{+/+}$ and *AnxA2*$^{-/-}$ BECs (blue). Endonuclease-treated sections and samples lacking TdT are positive and negative controls, respectively. (C,D) Cleaved caspase-3 activity (CC3, green) in *AnxA2*$^{+/+}$ (C) and *AnxA2*$^{-/-}$ (D) BECs labeled for E-cadherin (red) and nuclei (DAPI, blue). (E) Confocal images of cross-sections of *AnxA2*$^{+/+}$ and *AnxA2*$^{-/-}$ quadriceps muscle labeled for ANXA2 (red) and COL6 (green). (F) Adhesion of *AnxA2*$^{+/+}$ and *AnxA2*$^{-/-}$ mEFs to matrices. Attached cells were removed and expressed as a percentage of total cells plated (means ± s.e.; P<0.039 for comparison of *AnxA2*$^{-/-}$ cells on BSA alone versus BSA + COL6). Scale bars: 50 μm.

larger role in regulating secretion of additional matrix proteins that must undergo high-level intracellular assembly. Our unpublished data are consistent with this possibility, and indicate that at least one additional basement membrane protein, fibulin-2, is abnormally secreted. Because COL6 secretion involves a high level of pre-assembly that is not required for secretion of other collagens or most other matrix proteins, it is perhaps not surprising that COL6 must be prepackaged within specialized secretory vesicles (Bateman et al., 2009). COL6 is composed most often of three genetically distinct polypeptide chains (COL6a1, COL6a2 and COL6a3), which assemble intracellularly into monomers that form higher-order polymers (Furthmayr et al., 1983). Antiparallel pairing of monomers gives rise to disulfide-stabilized dimers, which then form 12-chain complexes. This extensive polymerization occurs prior to secretion within secretory vesicles (Colombatti and Bonaldo, 1987; Colombatti et al., 1995; Engvall et al., 1986) and mutations that perturb COL6 assembly, as in Bethlem myopathy, also prevent its secretion (Lamandé et al., 1999).

ANXA2 has been found to participate in the regulated exocytosis of at least three classes of molecules through interactions with SNARE proteins. During release of chromaffin granule-associated catecholamines, ANXA2 translocates in an S100A10-dependent manner to a SNARE protein complex, consisting of SNAP-25, VAMP2 and syntaxin, at points of plasma-membrane-secretory granule contact (Creutz et al., 1978; Umbrecht-Jenck et al., 2010). In the endothelial cell, ultralarge (~20,000 kDa) multimers of the procoagulant protein von Willebrand Factor (vWF) are pre-packaged within specialized structures, the Weibel–Palade bodies, and released by exocytosis in response to specific stimuli, such as thrombin, histamine or complement factors that trigger fusion with the plasma membrane (Pimanda and Hogg, 2002; Sadler, 2009). In primary cultures of endothelial cells, this process requires SNARE proteins, including SNAP-23, syntaxin 4 and VAMP3, as well as the annexin-A2–S100A10 heterotetramer (Knop et al., 2004; Rojo Pulido et al., 2011). In the lung, type II alveolar pneumocytes release surfactant, a complex of phospholipids and proteins SP-A and SP-D, upon fusion of lamellar bodies with the plasma membrane (Dietl et al., 2012). In this process, ANXA2 binds to SNAP-23 in a Ca^{2+}-dependent manner (Wang et al., 2007). Thus, it appears that ANXA2 might be among the diverse proteins that regulate or support SNARE-related exocytosis (Kasai et al., 2012; Rizo and Südhof, 2012).

In the biosynthetic-secretory pathway, proteins shuttle from the ER to the Golgi in 60–90 nm coat protein complex (COP)II-coated vesicles, and then from the Golgi to the plasma membrane in similar-sized COPI-coated vesicles, prior to vesicle fusion with the plasma membrane. However, to accommodate COL7, and possibly other collagens, which form 300–400 nm triple-helical rod-like 'monomers', proteins such as TANGO (transport and Golgi organization) and cTAGE5 (cutaneous T-cell lymphoma-associated antigen 5) appear to assemble at ER-exit sites and delay COPII membrane coating, resulting in larger-diameter vesicles (Malhotra and Erlmann, 2011). Our data suggest that an additional post-Golgi adaptation facilitates export of COL6, which undergoes even higher-level, tetrameric assembly. We propose a model in which intravesicular COL6 interacts with VAMP2, a transmembrane vesicular protein, which in turn interacts with extravesicular SNAP-23 and ANXA2. ANXA2 appears to enable plasma membrane docking of vesicles and/or fusion by interacting with SNAREs in the final step of COL6 secretion (Kasai et al., 2012). In the absence of ANXA2, membrane fusion fails and COL6 accumulates within VAMP2-positive late-Golgi vesicles, thus defying export. This mechanism might be unique to COL6, because COL1 and COL4 appear to be normally localized in the bronchial epithelial basement membrane of the *AnxA2*$^{-/-}$ mouse.

The high level of apoptosis in *AnxA2*$^{-/-}$ bronchial epithelial cells suggested cell loss that is due to anoikis, whereby disadhesion induces apoptotic cell death in anchorage-dependent cells (Chiarugi and Giannoni, 2008; Frisch and Screaton, 2001; Taddei et al., 2012). Interestingly, soluble COL6 appears to prevent apoptosis of serum-starved fibroblasts by suppressing the pro-apoptotic protein, Bax (Rühl et al., 1999). In avian corneal fibroblasts, cell viability depends specifically on the interaction between matrix-associated COL6 and cell-membrane-associated β1 integrins (Howell and Doane, 1998), and COL6 also appears to protect chondrocytes, neurons and cardiac myocytes from apoptosis due to chemical inducers, ultraviolet irradiation or early, but not late, tissue infarction, respectively (Cheng et al., 2011; Luther et al., 2012; Peters et al., 2011). In *Col6a1*$^{-/-}$ mice, myofibers undergo apoptotic cell death in a process thought to reflect opening of the cyclosporine-A-sensitive, mitochondrial permeability transition pore, which might be triggered by integrin-mediated induction of reactive oxygen species or defective regulation of autophagy (Grumati et al., 2010; Irwin et al., 2003).

In our studies in the *AnxA2*$^{-/-}$ mouse, changes in bronchiolar epithelial cells were among the most dramatic pulmonary findings. These cells displayed a dense, flattened appearance, a high apoptotic index and a striking reduction in the proportion of ciliated cells, possibly indicating replacement by Clara-like progenitor cells. Further studies confirmed dropout of airway epithelial cells in response to bronchoalveolar lavage, and experiments with embryonic fibroblasts revealed impaired adhesion of cells of either genotype to *AnxA2*$^{-/-}$ mEF-derived matrix. Impaired adhesion of *AnxA2*$^{-/-}$ mEFs to albumin–matrix substrate could be restored to the level seen for *AnxA2*$^{+/+}$ mEFs by addition of COL6. This is a finding consistent with previous studies, indicating that cellular adhesion to COL6 is dependent upon β_1 integrins (Pfaff et al., 1993). Furthermore, the COL6-related loss of cells secreting basement membrane could compromise deposition of additional normal matrix proteins that contribute to normal pulmonary compliance and elastance. In summary, our data show that ANXA2 is fundamental to secretion of COL6, subsequent cell adhesion to basement membrane, prevention of apoptotic cell dropout and normal pulmonary function.

Journal of Cell Science (2014) 127, 828–844 doi:10.1242/jcs.137802

MATERIALS AND METHODS

Mice

AnxA2$^{-/-}$ and *AnxA2*$^{+/+}$ mice were generated by homologous recombination as described previously (Ling et al., 2004). Either littermate pairs or mice cross-bred extensively to the C57BL/6 background were used. *Col6a1*$^{-/-}$ mice, which lack α chain expression and fail to form triple-helical COL6 monomers, were generated as described and bred to a mixed FVB-C57BL/6 background (Bonaldo et al., 1998). All animal procedures were performed in accordance with Institutional Animal Care and Use Committee approval.

Exercise testing

Swim testing took place in a plexiglass tank containing stationary room-temperature (23±1℃) water at a depth of 20 cm. After swimming, mice were placed in cages containing normal bedding and maintained at 21℃. *AnxA2*$^{-/-}$ and *AnxA2*$^{+/+}$ littermate mice underwent a 3 week training period consisting of supervised swim sessions 4–5 times per week and increasing in duration by 10 minute intervals to a plateau of 90 minutes per session (Godínez-Victoria et al., 2012; Kregel et al., 2006). Thereafter, mice were subjected to 90 minute daily swim sessions over a 3 week period. Recovery time, defined as duration from removal from the swim tank to the time of complete coat dryness, was recorded by a masked observer (Meeks and Larson, 2012). At the conclusion of each experiment, the mice were sacrificed and heart to body weight ratios determined.

Cardiac evaluation

After 3 days of acclimatization to handling, prewarmed ultrasound gel was applied to the depilated anterior chest of seven *AnxA2*$^{-/-}$ and seven *AnxA2*$^{+/+}$ mice (Donovan et al., 2000). An Acuson Sequoia™ C512 15-MHz linear array probe (Siemens Medical Solutions, Malvern, PA) was placed on the anterior chest wall and the position of the transducer confirmed using two-dimensional long- or short-axis images. An M-mode cursor was then placed at the level of the papillary muscles and M-modes recorded at a sweep speed of 200 cm/second. Left ventricular dimensions in diastole (*LVIDd*) and systole (*LVIDs*), as well as septal and posterior wall thickness and heart rate, were measured over four to six cycles using the Digisonics Offline Analysis System. Left ventricular volumes in diastole (*VolD*) and systole (*VolS*) were calculated using a cubed formula. Fractional shortening was calculated using the formula, $FS\ (\%) = 100 \times (LVIDd\text{-}LVIDs)/LVIDd$. Stroke volume (*SV*) was calculated as the difference between VolD and VolS. Ejection fraction (*EF*) was calculated using the formula: $EF\ (\%) = 100 \times (VolD - VolS)/VolD$. Cardiac output was derived from the formula $SV \times HR$. Left ventricular mass was calculated using the prolate ellipse formula (Lang et al., 2005).

Pulmonary biomechanics

Respiratory mechanics were evaluated on anaesthetized mice (125 mg/kg pentobarbital, 15 mg/kg xylazine; i.p.) that were tracheostomized and mechanically ventilated using a computer-controlled animal ventilator (Sireq, Montreal, Canada). Three perturbations were used to assess baseline respiratory mechanics and were analyzed using Flexivent software (Scireq). Static compliance was determined using the Salazar–Knowles equation to the plateau pressure measurements obtained between total lung capacity and functional residual capacity. Single-frequency forced oscillations were used to determine tissue resistance (*R*), elastance (*E*) and dynamic compliance (*C*) using a single compartment model. Broadband forced oscillations served to determine Newtonian (airway) resistance (R_n), tissue dampening (*G*) and tissue elastance (*H*) using a constant phase model. R_n was also assessed following increasing doses of nebulized methacholine (3.125, 12.5 and 50 mg/ml). Inspiratory capacity was determined between the plateau pressure measurements of the total lung capacity and functional residual volume (Ding et al., 2011).

Tissue processing and histology

Sections were initially stained with hematoxylin and eosin. Unstained sections were also imaged by autofluorescence using a green FITC-filter channel and UV excitation. For immunohistology, 4% paraformaldehyde (PFA)-fixed frozen lung sections were treated with blocking solution (DPBS/5% BSA, 1 hour), and then incubated overnight in blocking solution containing rabbit polyclonal anti-human ANXA2 IgG (clone H-50; Santa Cruz Biotech), or containing goat polyclonal anti-mouse COL6 IgG (clone S-16; Santa Cruz Biotech). Samples were washed and incubated with donkey anti-rabbit or anti-goat IgG coupled to Cy3, Alexa Fluor 569 or Alexa Fluor 647 (Jackson Immunochemicals and Invitrogen). Coverslips were mounted with Vectashield mounting medium (Vector Laboratories, Inc., Burlingame, CA). Mounted coverslips were imaged by fluorescence microscopy (Retiga 1300i), or by confocal microscopy (Zeiss LSM 5 Live). For immunochemistry, 4% PFA-fixed frozen lung tissue sections were treated as above, and incubated with secondary donkey anti-rabbit or anti-goat peroxidase-conjugated antibodies (blocking solution, 1 hour), rinsed, and counterstained with DAPI.

For detection of apoptosis, *in situ* terminal deoxynucleotidyl transferase-mediated DNA nick-end labeling (TdT-TUNEL) staining was performed using the TACS 2 *in situ* kit (Trevigen Inc., Gaithersburg, MD). Briefly, fixed lung sections were incubated with TdT Blue labeling buffer (0.01% Thimerasol, 0.5% BSA, <0.01% 2-mercaptoethanesulfonic acid, TES sodium salt, pH 7.5; 5 minutes), followed by either labeling reagents (10 µM biotinylated dNTP, terminal deoxynucleotidyl transferase (TdT) enzyme, and Co^{2+} cation) or TACS-nuclease for positive controls (1 hour, 37℃). The reaction was stopped with termination buffer (10 mM EDTA, pH 8.0, 15 minutes, 21℃) and blue labeling of cell nuclei imaged. For identification of cleaved caspase-3 activity, fixed lung cryosections were blocked (5% BSA) and incubated with rabbit monoclonal anti-human activated caspase 3 (Cell Signaling), followed by polyclonal goat anti-E-cadherin IgG (R&D Systems). Secondary antibodies were Cy5-labeled goat anti-rabbit and Cy3-labeled donkey anti-goat IgG (Jackson Immunochemicals).

RT-PCR

RNA was extracted from lung tissue with Trizol (Invitrogen) and purified by standard phenol–chloroform and ethanol precipitation. To generate cDNAs from extracted RNA, reverse primers complementary to a portion of *Col6a1*, Col6*a2* and Col6*a3* were used in reverse transcriptase reactions. Semi-quantitative PCR was performed with the resulting cDNA templates, with primer pairs corresponding to exons 1 and 2 in *Col6a1 and Col6a2*, exons 1 and 3 in *Col6a3*, and Taq polymerase (Denville Scientific, NJ). Primers for GAPDH were used as internal controls (primer sequences available upon request). PCR cycles were as follows: 94℃, 5 minutes for denaturation, 32 cycles of 94℃, 1 minute; 59℃, 90 seconds for annealing; and 72℃, 2 minutes for extension. For real-time PCR, LightCycler 480 reaction mastermix was prepared according to the manufacturer's protocol (SYBR I Green Master; Roche Diagnostics) and added to 1 µl cDNA in individual wells of a 384-well plate. PCR cycles were as follows: 95℃ for 5 minutes (denaturation), 95℃ for 30 seconds, 60℃ for 30 seconds, 76℃ for 30 seconds (amplification and quantification) for 40 cycles, 60℃–95℃ with a heating rate of 0.1℃ per second and a continuous fluorescence measurement (melting curve) and 40℃ (final cooling). Relative expression ratios were determined by 'Fit Point Method,' using LightCycler 480 Software (Roche Diagnostics) (Pfaffl, 2001).

Immunoblot analysis

Protein samples were analyzed on 12.5% SDS-polyacrylamide gels. Proteins were transferred to nitrocellulose membranes (18 hours, 120 mA, 4℃), which were then blocked (5% milk, 1 hour, 21℃), and probed with rabbit polyclonal IgGs directed against ANXA2 (clone H-50; Santa Cruz Biotech), mouse tropoelastin (Abcam), human β-tubulin (Abcam), mouse SNAP23 (clone G-16) (Santa Cruz Biotech), rat VAMP2 (Abcam), rat syntaxin-2 (Abcam) or mouse monoclonal IgG directed against human β-actin (Santa Cruz Biotech). Membranes were developed with peroxidase-conjugated anti-rabbit and anti-goat IgGs (GE Healthcare), and ECL Plus detection reagents (GE Healthcare).

Cell culture and adenoviral infection

Primary cultures of mouse embryonic fibroblasts (mEFs) were established from E14.5 embryos that were rinsed with 1× PBS, minced

with a razor blade, and incubated in 0.1% trypsin, 1 mM EDTA (37℃, 15 minutes, gentle agitation). The resulting supernatant was centrifuged (200 ***g***, 5 minutes) and the pellet resuspended in prewarmed mEF medium (DMEM, 10% fetal bovine serum (FBS), 0.01% L-glutamine, 0.01% sodium pyruvate, and 0.01% penicillin-streptomycin). For transfection, mEFs were incubated with mouse cDNA expression plasmids encoding GFP-tagged versions of COL6 (accession no. NM_009933.4; OriGene, Rockville, MD) using TurboFectin 8.0 reagent (OriGene) per the manufacturer's guide. For adenoviral infection, mEFs were incubated with an adenoviral construct containing recombinant ANXA2 and a GFP marker (AdV-A2), or an empty GFP-encoding control vector (AdV-null), in serum-free mEF medium (2 hours, 37℃). Twenty-four hours post infection, fresh complete mEF medium was added, and cells incubated for 48 hours.

siRNA transfection

mEFs were transfected with either mock, SNAP-23- or VAMP2-directed siRNA (Santa Cruz Biotech) in siRNA Transfection Medium, as per the manufacturer's protocol (Santa Cruz Biotech). Five to seven hours later, complete medium containing twice the normal serum and antibiotic concentration was added. Twenty-four hours post transfection, the medium was replaced with normal growth medium, and the cells assayed 24 hours later.

Cell staining

For immunocytology, cells were fixed with 2% PFA and 2.5% sucrose in DPBS plus calcium and magnesium (C/M; 15 minutes, 37℃). Cells were blocked with either DPBS C/M plus MOM (Vector Laboratories) or DPBS C/M with 5% normal donkey serum, each containing 0.3 M glycine, and 0.1% Tween-20. Cells were blocked for 1 hour, and then incubated with primary antibody (2 hours, 37℃), or overnight in blocking solution plus primary antibody (supplementary material Table S2). Samples were washed and incubated with secondary antibody (supplementary material Table S3). Coverslips were mounted with Fluoromount G medium (Electron Microscopy Sciences, Hatfield, PA), and imaged by fluorescence (Retiga 1300i) or confocal microscopy (Zeiss LSM 5 Live). Fluorescence signals were quantified using Image J (1.48c, National Institutes of Health, USA).

Cell lysates

Mouse lungs were flash frozen in liquid N_2 and ground manually into a fine powder with a mortar and pestle. Washed, cultured cells were scraped and pelleted (200 *g*, 21℃). Pelleted cells or tissue powder was resuspended in lysis buffer [25 mM Tris-HCl, pH 7.5, 150 mM NaCl, 1 mM EDTA, 1% Triton X-100, 1 mM complete mini protease inhibitor cocktail (Roche), 1 mM DTT, 1 mM PMSF]. Lysates were passed sequentially through 26.5-, 28- and 30-gauge needles, nutated (4℃, 2 hours) and then centrifuged (16,060 ***g***, 4℃, 15 minutes) for collection of supernatants. Pellets containing Triton-X-insoluble proteins were extracted with ECM buffer (8 M urea, 500 mM NaCl, 50 mM Tris-HCl, pH 7.5, 0.5% Triton X-100, 1 mM complete mini protease inhibitor cocktail, 0.02 mM PMSF). Protein concentrations were estimated using the bicinchoninic acid assay (BCA).

Subcellular fractionation

Flash-frozen mouse lungs were Dounce-homogenized (30 strokes, conical microcentrifuge pestle, Thomas Scientific) in cell extraction buffer (50 mM Tris-HCl, pH 7.3, 250 mM sucrose, 2 mM EDTA, 2 mM protease inhibitor cocktail), and centrifuged twice (2800 ***g***, 4℃, 20 minutes) to remove unbroken cells and nuclei. Ice-cold aqueous 0.1 M Na_2CO_3 (pH 11) was added to the supernatant homogenate and agitated gently (4℃, 1 hour), prior to two additional centrifugations (100,000 ***g***, 1 hour, 4℃). Pooled supernatants (cytosol) and pellets (microsomes) were resuspended in cell extraction buffer containing 8 M urea and analyzed by immunoblot.

Immunoprecipitation

Protein extracts (750 µg) from whole-lung homogenates were mixed with pre-washed protein A/G beads (Santa Cruz Biotech), resuspended at 100 µg/µl and coupled with 10 µg of rabbit polyclonal anti-human COL6 (Rockland) or rabbit polyclonal anti-human ANXA2 antibodies (Santa Cruz Biotech) and incubated (5 hours, 4℃). Immunocomplexes were washed four times with cell lysis buffer and once with DPBS, and then analyzed by immunoblot.

Trypsin protection assay

Microsomes (75 µg) underwent limited digestion with trypsin (Worthington, 0.1 µg/ml, 24℃, 60 min) (Sarkadi et al., 1986). Reactions were quenched with 1 mM protease inhibitor cocktail and 1 mM PMSF. Untreated and trypsin-treated samples were analyzed by SDS-PAGE and immunoblot.

Immunoelectron microscopy

To determine areas of interest for electron microscopy imaging, ultra-thin 1.0 µm tissue sections were fixed in 4% PFA and 0.1% glutaraldehyde in DPBS (Cellgro, Manassas, Virginia), stained with Toluidine Blue, rinsed with dH_20 and imaged by brightfield microscopy (Retiga 1300i). For electron microscopy imaging, the sections were post-fixed in 1% OsO_4, contrasted in 1% uranyl acetate, dehydrated and embedded in acrylic resin. For immunogold labeling, ultrathin sections were transferred to grids, incubated with either primary polyclonal rabbit anti-human ANXA2 IgG or goat anti-human ANXA2 IgG (Santa Cruz Biotech), goat anti-mouse COL6 (Santa Cruz Biotech), goat anti-human SNAP-23 (Santa Cruz Biotech) or rabbit anti-rat VAMP2 (Abcam) in various combinations, and incubated with anti-rabbit 10-nm-gold-conjugated and anti-goat 6-nm-gold-conjugated antibodies (Aurion). Grids were examined in a JEM 1400 transmission electron microscope (JEOL Ltd, Japan).

Bronchoalveolar lavage

PBS (0.5 ml) was delivered via endotracheal tube and then immediately withdrawn using gentle suction. This procedure was repeated once, and the recovered fluid, typically ~600 µl, pooled and stained with Trypan Blue for total cell counts in a hemocytometer. Differential counts were performed on cytospins stained with Diff-Quik (Dade Behring, Düdingen, Switzerland); at least 500 cells were evaluated for each preparation (Walters et al., 2000).

Cell-adhesion assay

Biosynthesized ECM was prepared by incubating *AnxA2*$^{+/+}$ and *AnxA2*$^{-/-}$ mEFs on BSA-coated wells (8 hours, 37℃, 5% CO_2), with prewarmed mEF medium) until confluent. The cells were washed with 1 ml PBS C/M, treated with 1 ml lysis buffer (0.5% Triton X-100, 0.02 M NH_4OH), and rinsed once with PBS C/M before use. To evaluate cell adhesion, mEFs were plated (~50,000 cells/well, 24-well plates, 8 hours) on uncoated polystyrene wells or wells coated with BSA, COL6 (Abcam) or biosynthetic ECM (Rickard et al., 1991). The supernatant medium was then removed, and unattached cells counted by hemocytometer. Attached cells were rinsed once with PBS C/M to remove loosely attached cells, collected after incubation with 1 ml 0.25% trypsin in EDTA (Cellgro; 2 minutes, 37℃), and counted.

Statistical analyses

Graphs and associated statistics were generated with GraphPad Prism software (v. 4.00, San Diego, CA) and Microsoft Excel 2007. Data are provided as mean ± s.e. Significance of differences was calculated using the Student's unpaired *t*-test.

Acknowledgements

We thank Ralph L. Nachman, Biin Sung, Andrew T. Jacovina, and Lee Cohen-Gould and Becky Smith for helpful discussions and assistance with pulmonary mechanics, exercise testing, and immunoelectron microscopy, respectively.

Author contributions

M.D. jointly conceived the study, carried out experiments, analyzed data and co-wrote the manuscript. D.A. performed the immunostaining and microscopy. R.H. performed echocardiography studies. P.B. provided COL6A1-null mice. S.W.

planned and analyzed the pulmonary function tests. K.A.H. jointly conceived the study, supervised the project, and co-wrote the manuscript. All authors discussed the results, implications, and commented on the manuscript at all stages.

Competing interests

Thea authors declare no competing interests.

Funding

This research was supported by the National Institutes of Health [grant numbers HL042493, HL046403 and HL090895 to K.A.H.; T32-HL007423-30 to M.D.]; the March of Dimes [grant number 6-FY12-356 to K.A.H.]; and a Hartwell Foundation Postdoctoral Fellowship to M.D. Deposited in PMC for release after 12 months.

Supplementary material

Supplementary material available online at
http://jcs.biologists.org/lookup/suppl/doi:10.1242/jcs.137802/-/DC1

References

Baker, N. L., Mörgelin, M., Peat, R., Goemans, N., North, K. N., Bateman, J. F. and Lamandé, S. R. (2005). Dominant collagen VI mutations are a common cause of Ullrich congenital muscular dystrophy. *Hum. Mol. Genet.* **14**, 279-293.

Bateman, J. F., Boot-Handford, R. P. and Lamandé, S. R. (2009). Genetic diseases of connective tissues: cellular and extracellular effects of ECM mutations. *Nat. Rev. Genet.* **10**, 173-183.

Bober, M., Enochsson, C., Collin, M. and Mörgelin, M. (2010). Collagen VI is a subepithelial adhesive target for human respiratory tract pathogens. *J. Innate Immun.* **2**, 160-166.

Bonaldo, P., Russo, V., Bucciotti, F., Doliana, R. and Colombatti, A. (1990). Structural and functional features of the alpha 3 chain indicate a bridging role for chicken collagen VI in connective tissues. *Biochemistry* **29**, 1245-1254.

Bonaldo, P., Braghetta, P., Zanetti, M., Piccolo, S., Volpin, D. and Bressan, G. M. (1998). Collagen VI deficiency induces early onset myopathy in the mouse: an animal model for Bethlem myopathy. *Hum. Mol. Genet.* **7**, 2135-2140.

Bönnemann, C. G. (2011). The collagen VI-related myopathies: muscle meets its matrix. *Nat. Rev. Neurol* **7**, 379-390.

Cheng, I. H., Lin, Y. C., Hwang, E., Huang, H. T., Chang, W. H., Liu, Y. L. and Chao, C. Y. (2011). Collagen VI protects against neuronal apoptosis elicited by ultraviolet irradiation via an Akt/phosphatidylinositol 3-kinase signaling pathway. *Neuroscience* **183**, 178-188.

Chiarugi, P. and Giannoni, E. (2008). Anoikis: a necessary death program for anchorage-dependent cells. *Biochem. Pharmacol.* **76**, 1352-1364.

Colombatti, A. and Bonaldo, P. (1987). Biosynthesis of chick type VI collagen. II. Processing and secretion in fibroblasts and smooth muscle cells. *J. Biol. Chem.* **262**, 14461-14466.

Colombatti, A., Mucignat, M. T. and Bonaldo, P. (1995). Secretion and matrix assembly of recombinant type VI collagen. *J. Biol. Chem.* **270**, 13105-13111.

Cox, T. R. and Erler, J. T. (2011). Remodeling and homeostasis of the extracellular matrix: implications for fibrotic diseases and cancer. *Dis. Model. Mech.* **4**, 165-178.

Creutz, C. E., Pazoles, C. J. and Pollard, H. B. (1978). Identification and purification of an adrenal medullary protein (synexin) that causes calcium-dependent aggregation of isolated chromaffin granules. *J. Biol. Chem.* **253**, 2858-2866.

Dassah, M., Deora, A. B., He, K. and Hajjar, K. A. (2009). The endothelial cell annexin A2 system and vascular fibrinolysis. *Gen. Physiol. Biophys.* **28 Spec. No Focus**, F20-F28.

Dietl, P., Haller, T. and Frick, M. (2012). Spatio-temporal aspects, pathways and actions of Ca(2+) in surfactant secreting pulmonary alveolar type II pneumocytes. *Cell Calcium* **52**, 296-302.

Ding, B. S., Nolan, D. J., Guo, P., Babazadeh, A. O., Cao, Z., Rosenwaks, Z., Crystal, R. G., Simons, M., Sato, T. N., Worgall, S. et al. (2011). Endothelial-derived angiocrine signals induce and sustain regenerative lung alveolarization. *Cell* **147**, 539-553.

Donovan, M. J., Lin, M. I., Wiegn, P., Ringstedt, T., Kraemer, R., Hahn, R., Wang, S., Ibañez, C. F., Rafii, S. and Hempstead, B. L. (2000). Brain derived neurotrophic factor is an endothelial cell survival factor required for intramyocardial vessel stabilization. *Development* **127**, 4531-4540.

Engvall, E., Hessle, H. and Klier, G. (1986). Molecular assembly, secretion, and matrix deposition of type VI collagen. *J. Cell Biol.* **102**, 703-710.

Evans, M. J., Van Winkle, L. S., Fanucchi, M. V., Toskala, E., Luck, E. C., Sannes, P. L. and Plopper, C. G. (2000). Three-dimensional organization of the lamina reticularis in the rat tracheal basement membrane zone. *Am. J. Respir. Cell Mol. Biol.* **22**, 393-397.

Flood, E. C. and Hajjar, K. A. (2011). The annexin A2 system and vascular homeostasis. *Vascul. Pharmacol.* **54**, 59-67.

Frisch, S. M. and Screaton, R. A. (2001). Anoikis mechanisms. *Curr. Opin. Cell Biol.* **13**, 555-562.

Furthmayr, H., Wiedemann, H., Timpl, R., Odermatt, E. and Engel, J. (1983). Electron-microscopical approach to a structural model of intima collagen. *Biochem. J.* **211**, 303-311.

Gelse, K., Pöschl, E. and Aigner, T. (2003). Collagens – structure, function, and biosynthesis. *Adv. Drug Deliv. Rev.* **55**, 1531-1546.

Gerke, V., Creutz, C. E. and Moss, S. E. (2005). Annexins: linking Ca2+ signalling to membrane dynamics. *Nat. Rev. Mol. Cell Biol.* **6**, 449-461.

Godínez-Victoria, M., Drago-Serrano, M. E., Reyna-Garfias, H., Viloria, M., Lara-Padilla, E., Resendiz-Albor, A. A., Sánchez-Torres, L. E., Cruz-Hernández, T. R. and Campos-Rodriguez, R. (2012). Effects on secretory IgA levels in small intestine of mice that underwent moderate exercise training followed by a bout of strenuous swimming exercise. *Brain Behav. Immun.* **26**, 1300-1309.

Grumati, P., Coletto, L., Sabatelli, P., Cescon, M., Angelin, A., Bertaggia, E., Blaauw, B., Urciuolo, A., Tiepolo, T., Merlini, L. et al. (2010). Autophagy is defective in collagen VI muscular dystrophies, and its reactivation rescues myofiber degeneration. *Nat. Med.* **16**, 1313-1320.

Howell, S. J. and Doane, K. J. (1998). Type VI collagen increases cell survival and prevents anti-beta 1 integrin-mediated apoptosis. *Exp. Cell Res.* **241**, 230-241.

Irwin, W. A., Bergamin, N., Sabatelli, P., Reggiani, C., Megighian, A., Merlini, L., Braghetta, P., Columbaro, M., Volpin, D., Bressan, G. M. et al. (2003). Mitochondrial dysfunction and apoptosis in myopathic mice with collagen VI deficiency. *Nat. Genet.* **35**, 367-371.

Kasai, H., Takahashi, N. and Tokumaru, H. (2012). Distinct initial SNARE configurations underlying the diversity of exocytosis. *Physiol. Rev.* **92**, 1915-1964.

Keene, D. R., Engvall, E. and Glanville, R. W. (1988). Ultrastructure of type VI collagen in human skin and cartilage suggests an anchoring function for this filamentous network. *J. Cell Biol.* **107**, 1995-2006.

Knop, M., Aareskjold, E., Bode, G. and Gerke, V. (2004). Rab3D and annexin A2 play a role in regulated secretion of vWF, but not tPA, from endothelial cells. *EMBO J.* **23**, 2982-2992.

Kranenburg, A. R., Willems-Widyastuti, A., Moori, W. J., Sterk, P. J., Alagappan, V. K. T., de Boer, W. I. and Sharma, H. S. (2006). Enhanced bronchial expression of extracellular matrix proteins in chronic obstructive pulmonary disease. *Am. J. Clin. Pathol.* **126**, 725-735.

Kregel, K. C., Allen, D. L., Booth, F. W., Fleshner, M. R., Henriksen, E. J., Musch, T. I., O'Leary, D. S., Parks, C. M., Poole, D. C., Ra'anan, A. W. et al. (2006). *Resource Book for the Design of Animal Exercise Protocols* (ed. K. C. Kregel). Bethesda, MD: American Physiological Society..

Lamandé, S. R., Shields, K. A., Kornberg, A. J., Shield, L. K. and Bateman, J. F. (1999). Bethlem myopathy and engineered collagen VI triple helical deletions prevent intracellular multimer assembly and protein secretion. *J. Biol. Chem.* **274**, 21817-21822.

Lambrecht, B. N. and Hammad, H. (2012). The airway epithelium in asthma. *Nat. Med.* **18**, 684-692.

Lang, R. M., Bierig, M., Devereux, R. B., Flachskampf, F. A., Foster, E., Pellikka, P. A., Picard, M. H., Roman, M. J., Seward, J., Shanewise, J. S. et al.; Chamber Quantification Writing Group; American Society of Echocardiography's Guidelines and Standards Committee; European Association of Echocardiography (2005). Recommendations for chamber quantification: a report from the American Society of Echocardiography's Guidelines and Standards Committee and the Chamber Quantification Writing Group, developed in conjunction with the European Association of Echocardiography, a branch of the European Society of Cardiology. *J. Am. Soc. Echocardiogr.* **18**, 1440-1463.

LeBleu, V. S., Macdonald, B. and Kalluri, R. (2007). Structure and function of basement membranes. *Exp. Biol. Med. (Maywood)* **232**, 1121-1129.

Ling, Q., Jacovina, A. T., Deora, A., Febbraio, M., Simantov, R., Silverstein, R. L., Hempstead, B., Mark, W. H. and Hajjar, K. A. (2004). Annexin II regulates fibrin homeostasis and neoangiogenesis in vivo. *J. Clin. Invest.* **113**, 38-48.

Lu, P., Takai, K., Weaver, V. M. and Werb, Z. (2011). Extracellular matrix degradation and remodeling in development and disease. *Cold Spring Harb. Perspect. Biol.* **3**, a005058-a005082.

Luther, D. J., Thodeti, C. K., Shamhart, P. E., Adapala, R. K., Hodnichak, C., Weihrauch, D., Bonaldo, P., Chilian, W. M. and Meszaros, J. G. (2012). Absence of type VI collagen paradoxically improves cardiac function, structure, and remodeling after myocardial infarction. *Circ. Res.* **110**, 851-856.

Malhotra, V. and Erlmann, P. (2011). Protein export at the ER: loading big collagens into COPII carriers. *EMBO J.* **30**, 3475-3480.

Manabe, R., Tsutsui, K., Yamada, T., Kimura, M., Nakanog, I., Shimono, C., Sanzen, N., Furutani, Y. Y., Fukuda, S. T., Oguri, Y. et al. (2008). Transcriptome-based systematic identification of extracellular matrix proteins. *Proc. Natl. Acad. Sci. USA* **105**, 12849-12854.

Meeks, A. and Larson, S. J. (2012). Evaluating fatigue in lupus-prone mice: preliminary assessments. *Pharmacol. Biochem. Behav.* **100**, 392-397.

Nadeau, A., Kinali, M., Main, M., Jimenez-Mallebrera, C., Aloysius, A., Clement, E., North, B., Manzur, A. Y., Robb, S. A., Mercuri, E. et al. (2009). Natural history of Ullrich congenital muscular dystrophy. *Neurology* **73**, 25-31.

Nakata, T., Sobue, K. and Hirokawa, N. (1990). Conformational change and localization of calpactin I complex involved in exocytosis as revealed by quick-freeze, deep-etch electron microscopy and immunocytochemistry. *J. Cell Biol.* **110**, 13-25.

Peters, H. C., Otto, T. J., Enders, J. T., Jin, W., Moed, B. R. and Zhang, Z. (2011). The protective role of the pericellular matrix in chondrocyte apoptosis. *Tissue Eng. Part A* **17**, 2017-2024.

Pfaff, M., Aumailley, M., Specks, U., Knolle, J., Zerwes, H. G. and Timpl, R. (1993). Integrin and Arg-Gly-Asp dependence of cell adhesion to the native and unfolded triple helix of collagen type VI. *Exp. Cell Res.* **206**, 167-176.

Pfaffl, M. W. (2001). A new mathematical model for relative quantification in real-time RT-PCR. *Nucleic Acids Res.* **29**, e45.
Pimanda, J. and Hogg, P. (2002). Control of von Willebrand factor multimer size and implications for disease. *Blood Rev.* **16**, 185-192.
Pozzi, A. and Zent, R. (2011). Extracellular matrix receptors in branched organs. *Curr. Opin. Cell Biol.* **23**, 547-553.
Proud, D. and Leigh, R. (2011). Epithelial cells and airway diseases. *Immunol. Rev.* **242**, 186-204.
Rickard, K. A., Shoji, S., Spurzem, J. R. and Rennard, S. I. (1991). Attachment characteristics of bovine bronchial epithelial cells to extracellular matrix components. *Am. J. Respir. Cell Mol. Biol.* **4**, 440-448.
Rizo, J. and Südhof, T. C. (2012). The membrane fusion enigma: SNAREs, Sec1/Munc18 proteins, and their accomplices – guilty as charged? *Annu. Rev. Cell Dev. Biol.* **28**, 279-308.
Rojo Pulido, I., Nightingale, T. D., Darchen, F., Seabra, M. C., Cutler, D. F. and Gerke, V. (2011). Myosin Va acts in concert with Rab27a and MyRIP to regulate acute von-Willebrand factor release from endothelial cells. *Traffic* **12**, 1371-1382.
Rühl, M., Sahin, E., Johannsen, M., Somasundaram, R., Manski, D., Riecken, E. O. and Schuppan, D. (1999). Soluble collagen VI drives serum-starved fibroblasts through S phase and prevents apoptosis via down-regulation of Bax. *J. Biol. Chem.* **274**, 34361-34368.
Sadler, J. E. (2009). von Willebrand factor assembly and secretion. *J. Thromb. Haemost.* **7 Suppl. 1**, 24-27.
Sarkadi, B., Enyedi, A., Földes-Papp, Z. and Gárdos, G. (1986). Molecular characterization of the in situ red cell membrane calcium pump by limited proteolysis. *J. Biol. Chem.* **261**, 9552-9557.
Specks, U., Nerlich, A., Colby, T. V., Wiest, I. and Timpl, R. (1995). Increased expression of type VI collagen in lung fibrosis. *Am. J. Respir. Crit. Care Med.* **151**, 1956-1964.
Taddei, M. L., Giannoni, E., Fiaschi, T. and Chiarugi, P. (2012). Anoikis: an emerging hallmark in health and diseases. *J. Pathol.* **226**, 380-393.
Telfer, W. R., Busta, A. S., Bonnemann, C. G., Feldman, E. L. and Dowling, J. J. (2010). Zebrafish models of collagen VI-related myopathies. *Hum. Mol. Genet.* **19**, 2433-2444.
Tooley, L. D., Zamurs, L. K., Beecher, N., Baker, N. L., Peat, R. A., Adams, N. E., Bateman, J. F., North, K. N., Baldock, C. and Lamandé, S. R. (2010). Collagen VI microfibril formation is abolished by an α2(VI) von Willebrand factor type A domain mutation in a patient with Ullrich congenital muscular dystrophy. *J. Biol. Chem.* **285**, 33567-33576.
Umbrecht-Jenck, E., Demais, V., Calco, V., Bailly, Y., Bader, M. F. and Chasserot-Golaz, S. (2010). S100A10-mediated translocation of annexin-A2 to SNARE proteins in adrenergic chromaffin cells undergoing exocytosis. *Traffic* **11**, 958-971.
van der Kooi, A. J., de Voogt, W. G., Bertini, E., Merlini, L., Talim, F. B., Ben Yaou, R., Urtziberea, A. and de Visser, M. (2006). Cardiac and pulmonary investigations in Bethlem myopathy. *Arch. Neurol.* **63**, 1617-1621.
Vishwanatha, J. K., Muns, G., Beckmann, J. D., Davis, R. G. and Rubinstein, I. (1995). Differential expression of annexins I and II in bovine bronchial epithelial cells. *Am. J. Respir. Cell Mol. Biol.* **12**, 280-286.
Walters, D. M., Wills-Karp, M. and Mitzner, W. (2000). Assessment of cellular profile and lung function with repeated bronchoalveolar lavage in individual mice. *Physiol. Genomics* **2**, 29-36.
Wang, P., Chintagari, N. R., Gou, D., Su, L. and Liu, L. (2007). Physical and functional interactions of SNAP-23 with annexin A2. *Am. J. Respir. Cell Mol. Biol.* **37**, 467-476.
Zou, Y., Zhang, R. Z., Sabatelli, P., Chu, M. L. and Bönnemann, C. G. (2008). Muscle interstitial fibroblasts are the main source of collagen VI synthesis in skeletal muscle: implications for congenital muscular dystrophy types Ullrich and Bethlem. *J. Neuropathol. Exp. Neurol.* **67**, 144-154.